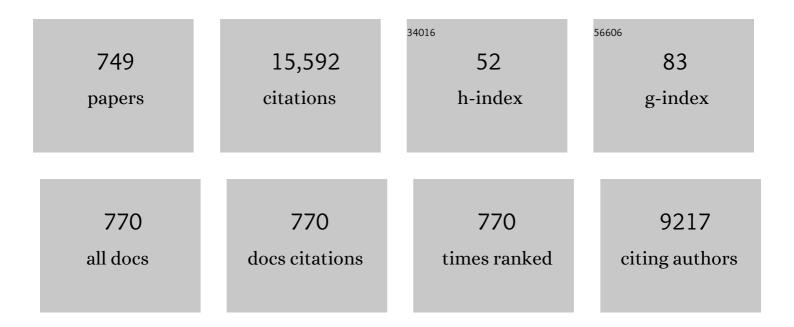


List of Publications by Year in descending order

Source: https://exaly.com/author-pdf/4400563/publications.pdf Version: 2024-02-01



#	Article	IF	CITATIONS
1	Diffusion coefficients of some solutes in fcc and liquid Al: critical evaluation and correlation. Materials Science & Engineering A: Structural Materials: Properties, Microstructure and Processing, 2003, 363, 140-151.	2.6	712
2	One-pot synthesized molybdenum dioxide–molybdenum carbide heterostructures coupled with 3D holey carbon nanosheets for highly efficient and ultrastable cycling lithium-ion storage. Journal of Materials Chemistry A, 2019, 7, 13460-13472.	5.2	220
3	Mesoporous metal–organic frameworks: design and applications. Energy and Environmental Science, 2012, 5, 7508.	15.6	203
4	Thermal stability and oxidation resistance of Ti–Al–N coatings. Surface and Coatings Technology, 2012, 206, 2954-2960.	2.2	202
5	A thermodynamic description of the Al–Fe–Si system over the whole composition and temperature ranges via a hybrid approach of CALPHAD and key experiments. Intermetallics, 2008, 16, 554-570.	1.8	177
6	Phase Equilibria and Thermodynamic Properties in the Fe-Cr System. Critical Reviews in Solid State and Materials Sciences, 2010, 35, 125-152.	6.8	172
7	Experimental Investigation and Thermodynamic Calculation of the Titanium–Silicon–Carbon System. Journal of the American Ceramic Society, 2000, 83, 197-203.	1.9	161
8	Exploring the size effects of Al4C3 on the mechanical properties and thermal behaviors of Al-based composites reinforced by SiC and carbon nanotubes. Carbon, 2018, 135, 224-235.	5.4	147
9	Effect of the second phases on corrosion behavior of the Mg-Al-Zn alloys. Journal of Alloys and Compounds, 2017, 695, 2330-2338.	2.8	145
10	Improving the mechanical properties of carbon nanotubes reinforced pure aluminum matrix composites by achieving non-equilibrium interface. Materials and Design, 2017, 120, 56-65.	3.3	142
11	Structural and elastic properties of cubic and hexagonal TiN and AlN from first-principles calculations. Computational Materials Science, 2010, 48, 705-709.	1.4	126
12	Liquid acid-catalysed fabrication of nanoporous 1,3,5-triazine frameworks with efficient and selective CO2 uptake. Polymer Chemistry, 2014, 5, 3424.	1.9	112
13	Facile Preparation of Dibenzoheterocycle-Functional Nanoporous Polymeric Networks with High Gas Uptake Capacities. Macromolecules, 2014, 47, 2875-2882.	2.2	108
14	CSUTDCC1—A thermodynamic database for multicomponent cemented carbides. International Journal of Refractory Metals and Hard Materials, 2014, 42, 57-70.	1.7	107
15	Reassessment of the Al–Mn system and a thermodynamic description of the Al–Mg–Mn system. International Journal of Materials Research, 2007, 98, 855-871.	0.1	106
16	Experimental investigations and thermodynamic descriptions of the Ni-Si and C-Ni-Si systems. Metallurgical and Materials Transactions A: Physical Metallurgy and Materials Science, 1999, 30, 2409-2418.	1.1	105
17	Influence of Zr on structure, mechanical and thermal properties of Ti–Al–N. Thin Solid Films, 2011, 519, 5503-5510.	0.8	102
18	Thermodynamic assessment of the Alî—,Ni system. Journal of Alloys and Compounds, 1996, 237, 20-32.	2.8	96

Үомс Du

#	Article	IF	CITATIONS
19	A pragmatic method to determine the composition-dependent interdiffusivities in ternary systems by using a single diffusion couple. Scripta Materialia, 2014, 90-91, 53-56.	2.6	94
20	Atomic mobilities and diffusivities in the fcc, L1 ₂ and B2 phases of the Ni-Al system. International Journal of Materials Research, 2010, 101, 1461-1475.	0.1	91
21	Thermodynamic properties of the Al–Fe–Ni system acquired via a hybrid approach combining calorimetry, first-principles and CALPHAD. Acta Materialia, 2009, 57, 5324-5341.	3.8	90
22	An overview on phase equilibria and thermodynamic modeling in multicomponent Al alloys: Focusing on the Al–Cu–Fe–Mg–Mn–Ni–Si–Zn system. Calphad: Computer Coupling of Phase Diagrams and Thermochemistry, 2011, 35, 427-445.	0.7	90
23	Effect of the modulation ratio on the interface structure of TiAlN/TiN and TiAlN/ZrN multilayers: First-principles and experimental investigations. Acta Materialia, 2017, 130, 281-288.	3.8	88
24	Diffusivities of an Al–Fe–Ni melt and their effects on the microstructure during solidification. Acta Materialia, 2010, 58, 3664-3675.	3.8	86
25	Quantified contribution of β″ and β′ precipitates to the strengthening of an aged Al–Mg–Si alloy. Materials Science & Engineering A: Structural Materials: Properties, Microstructure and Processing, 2020, 774, 138776.	2.6	84
26	Microstructures and mechanical properties of carbon nanotubes reinforced pure aluminum composites synthesized by spark plasma sintering and hot rolling. Materials Science & Engineering A: Structural Materials: Properties, Microstructure and Processing, 2017, 698, 282-288.	2.6	82
27	Enhanced mechanical properties of aluminum based composites reinforced by chemically oxidized carbon nanotubes. Carbon, 2018, 139, 459-471.	5.4	82
28	First-principles calculations of binary Al compounds: Enthalpies of formation and elastic properties. Calphad: Computer Coupling of Phase Diagrams and Thermochemistry, 2011, 35, 562-573.	0.7	81
29	Incorporating the CALPHAD sublattice approach of ordering into the phase-field model with finite interface dissipation. Acta Materialia, 2015, 88, 156-169.	3.8	81
30	Thermodynamic Assessment of the ZrO2YO1.5 System. Journal of the American Ceramic Society, 1991, 74, 1569-1577.	1.9	77
31	The influence of age-hardening on turning and milling performance of Ti–Al–N coated inserts. Surface and Coatings Technology, 2008, 202, 5158-5161.	2.2	76
32	Ca-decorated novel boron sheet: A potential hydrogen storage medium. International Journal of Hydrogen Energy, 2016, 41, 5276-5283.	3.8	76
33	Machining performance of Ti–Al–Si–N coated inserts. Surface and Coatings Technology, 2010, 205, 582-586.	2.2	73
34	Enhancement of strength and ductility by interfacial nano-decoration in carbon nanotube/aluminum matrix composites. Carbon, 2020, 159, 201-212.	5.4	73
35	On the constitution of the ternary system Al–Ni–Ti. Intermetallics, 2007, 15, 1257-1267.	1.8	72
36	Atomic scale investigation of the crystal structure and interfaces of the B′ precipitate in Al-Mg-Si alloys. Acta Materialia. 2020. 185. 193-203.	3.8	72

#	Article	IF	CITATIONS
37	Atomic mobilities, diffusivities and simulation of diffusion growth in the Co–Si system. Acta Materialia, 2008, 56, 3940-3950.	3.8	69
38	Thermodynamic description of the Al–Mg–Si system using a new formulation for the temperature dependence of the excess Gibbs energy. Thermochimica Acta, 2012, 527, 131-142.	1.2	68
39	Thermal stability and oxidation resistance of sputtered Ti Al Cr N hard coatings. Surface and Coatings Technology, 2017, 324, 48-56.	2.2	68
40	Machine learning reveals the importance of the formation enthalpy and atom-size difference in forming phases of high entropy alloys. Materials and Design, 2020, 193, 108835.	3.3	68
41	Compositional and structural evolution of sputtered Ti-Al-N. Thin Solid Films, 2009, 517, 6635-6641.	0.8	67
42	Structure and thermal properties of TiAlN/CrN multilayered coatings with various modulation ratios. Surface and Coatings Technology, 2016, 304, 512-518.	2.2	67
43	Nitrogen-doped porous carbons with high performance for hydrogen storage. International Journal of Hydrogen Energy, 2016, 41, 8489-8497.	3.8	65
44	Effects of Cu and Al on the crystal structure and composition of Î∙ (MgZn2) phase in over-aged Al–Zn–Mg–Cu alloys. Journal of Materials Science, 2012, 47, 5419-5427.	1.7	64
45	Atomistic structure of Cu-containing β″ precipitates in an Al–Mg–Si–Cu alloy. Scripta Materialia, 2014, 75, 86-89.	2.6	63
46	Thermodynamic Calculation of the Zirconia-Calcia System. Journal of the American Ceramic Society, 1992, 75, 3040-3048.	1.9	61
47	Thermal and thermo-mechanical properties of Ti–Al–N and Cr–Al–N coatings. International Journal of Refractory Metals and Hard Materials, 2012, 35, 235-240.	1.7	61
48	Mechanical properties, thermal stability and oxidation resistance of TiN/CrN multilayer coatings. Vacuum, 2020, 179, 109468.	1.6	61
49	Phase stability of magnesium-rare earth binary systems from first-principles calculations. Journal of Alloys and Compounds, 2011, 509, 6899-6907.	2.8	59
50	Effect of Si addition on microstructure and mechanical properties of Ti–Al–N coating. International Journal of Refractory Metals and Hard Materials, 2010, 28, 593-596.	1.7	58
51	Atomic mobilities, uphill diffusion and proeutectic ferrite growth in Fe–Mn–C alloys. Calphad: Computer Coupling of Phase Diagrams and Thermochemistry, 2009, 33, 614-623.	0.7	57
52	Thermodynamic assessment of the Mo–Nb–Ta system. Calphad: Computer Coupling of Phase Diagrams and Thermochemistry, 2004, 28, 133-140.	0.7	56
53	Improved properties of TiAlN coating by combined Si-addition and multilayer architecture. Journal of Alloys and Compounds, 2019, 790, 909-916.	2.8	55
54	Experimental reinvestigation of the CrSi-Si partial system and update of the thermodynamic description of the entire Cr-Si system. Journal of Phase Equilibria and Diffusion, 2000, 21, 281-286.	0.3	54

#	Article	IF	CITATIONS
55	Elastic constants of B2-MgRE (REÂ= ÂSc, Y, La–Lu) calculated with first-principles. Solid State Communications, 2008, 148, 314-318.	0.9	54
56	Phase-field simulation of diffusion couples in the Ni–Al system. International Journal of Materials Research, 2011, 102, 371-380.	0.1	54
5 7	Microstructure, mechanical and thermal properties of TiAlN/CrAlN multilayer coatings. International Journal of Refractory Metals and Hard Materials, 2013, 40, 51-57.	1.7	54
58	Formation enthalpies of Fe–Al–RE ternary alloys calculated with a geometric model and Miedema's theory. Journal of Alloys and Compounds, 2006, 416, 148-154.	2.8	53
59	Effect of bilayer period on structure, mechanical and thermal properties of TiAlN/AlTiN multilayer coatings. Thin Solid Films, 2015, 592, 207-214.	0.8	52
60	Mechanical properties and microstructural evolution of TiN coatings alloyed with Al and Si. Materials Science & Engineering A: Structural Materials: Properties, Microstructure and Processing, 2009, 502, 139-143.	2.6	51
61	Effect of CrN addition on the structure, mechanical and thermal properties of Ti-Al-N coating. Surface and Coatings Technology, 2013, 235, 506-512.	2.2	51
62	Ameliorated mechanical and thermal properties of SiC reinforced Al matrix composites through hybridizing carbon nanotubes. Materials Characterization, 2018, 136, 272-280.	1.9	51
63	Experimental investigation and thermodynamic description of the Co–Si system. Calphad: Computer Coupling of Phase Diagrams and Thermochemistry, 2006, 30, 470-481.	0.7	50
64	Mechanical properties of (Ti, Al)N monolayer and TiN/(Ti, Al)N multilayer coatings. International Journal of Refractory Metals and Hard Materials, 2007, 25, 72-76.	1.7	50
65	Improved thermal stability and oxidation resistance of Al–Ti–N coating by Si addition. Thin Solid Films, 2014, 556, 369-375.	0.8	50
66	Phase equilibria of the Al–Fe–Ni system at 850°C and 627°C. Journal of Alloys and Compounds, 2008, 454, 129-135.	2.8	49
67	Evolution of the microstructure and hardness of the Ti–Si alloys during high temperature heat-treatment. Journal of Alloys and Compounds, 2009, 479, 246-251.	2.8	49
68	Mechanical properties, thermal stability and oxidation resistance of Ta-doped CrAlN coatings. Surface and Coatings Technology, 2019, 368, 25-32.	2.2	49
69	A thermodynamic reassessment of the Al–Y system. Calphad: Computer Coupling of Phase Diagrams and Thermochemistry, 2006, 30, 334-340.	0.7	48
70	Experimental investigation of the Al–Y phase diagram. Journal of Alloys and Compounds, 2006, 414, 60-65.	2.8	48
71	A comparative research on physical and mechanical properties of (Ti, Al)N and (Cr, Al)N PVD coatings with high Al content. International Journal of Refractory Metals and Hard Materials, 2007, 25, 400-404.	1.7	47
72	Ab initio calculations and thermodynamic modeling for the Fe–Mn–Nb system. Calphad: Computer Coupling of Phase Diagrams and Thermochemistry, 2012, 38, 43-58.	0.7	46

#	Article	IF	CITATIONS
73	Viscosity and diffusivity in melts: from unary to multicomponent systems. Philosophical Magazine, 2014, 94, 1552-1577.	0.7	46
74	Shearing and rotation of β″ and βʹ precipitates in an Al-Mg-Si alloy under tensile deformation: In-situ and ex-situ studies. Acta Materialia, 2021, 220, 117310.	3.8	46
75	Refinement of the thermodynamic modeling of the Nb–Ni system. Calphad: Computer Coupling of Phase Diagrams and Thermochemistry, 2006, 30, 308-315.	0.7	45
76	Experimental investigation and thermodynamic modeling of the ternary Al–Cu–Fe system. Journal of Materials Research, 2009, 24, 3154-3164.	1.2	45
77	Thermodynamic investigation of the galvanizing systems, I: Refinement of the thermodynamic description for the Fe–Zn system. Calphad: Computer Coupling of Phase Diagrams and Thermochemistry, 2009, 33, 433-440.	0.7	44
78	Thermal conductivity of Al–Cu–Mg–Si alloys: Experimental measurement and CALPHAD modeling. Thermochimica Acta, 2016, 635, 8-16.	1.2	44
79	Effect of TaC and NbC addition on the microstructure and hardness in graded cemented carbides: Simulations and experiments. Ceramics International, 2016, 42, 428-435.	2.3	44
80	Ab initio calculation of the total energy and elastic properties of Laves phase C15 Al2RE (RE=Sc, Y, La,) Tj ETQq0 C)	Overlock 10 T
81	Assessment of atomic mobilities of Al and Cu in fcc Al–Cu alloys. Calphad: Computer Coupling of Phase Diagrams and Thermochemistry, 2009, 33, 761-768.	0.7	43
82	Thermal stability and oxidation resistance of V-alloyed TiAlN coatings. Ceramics International, 2018, 44, 1705-1710.	2.3	43
83	Thermodynamic modeling of the Mg–Si system with the Kaptay equation for the excess Gibbs energy of the liquid phase. Calphad: Computer Coupling of Phase Diagrams and Thermochemistry, 2009, 33, 673-678.	0.7	42
84	Hydrogen storage properties of destabilized MgH2–Li3AlH6 system. International Journal of Hydrogen Energy, 2010, 35, 8122-8129.	3.8	42
85	A coupled EBSD/TEM study of the microstructural evolution of multi-axial compressed pure Al and Al–Mg alloy. Materials Science & Engineering A: Structural Materials: Properties, Microstructure and Processing, 2016, 658, 16-27.	2.6	42
86	A new type of WC–Co–Ni–Al cemented carbide: Grain size and morphology of γ′-strengthened composi binder phase. Scripta Materialia, 2017, 126, 33-36.	ite 2.6	42
87	A thermodynamic description of the Al-Mn-Si system over the entire composition and temperature ranges. Metallurgical and Materials Transactions A: Physical Metallurgy and Materials Science, 2004, 35, 1613-1628.	1.1	41
88	Experimental investigation and thermodynamic modeling of the Al–Cu–Si system. Calphad: Computer Coupling of Phase Diagrams and Thermochemistry, 2009, 33, 200-210.	0.7	41
89	Atomic mobility, diffusivity and diffusion growth simulation for fcc Cu–Mn–Ni alloys. Calphad: Computer Coupling of Phase Diagrams and Thermochemistry, 2011, 35, 367-375.	0.7	41

90 Quantitative measurement for the microstructural parameters of nano-precipitates in Al-Mg-Si-Cu 1.9 41 alloys. Materials Characterization, 2016, 118, 352-362.

#	Article	IF	CITATIONS
91	Thermodynamic modeling of the V–Si system supported by key experiments. Calphad: Computer Coupling of Phase Diagrams and Thermochemistry, 2008, 32, 320-325.	0.7	40
92	Enthalpies of formation for the Al–Cu–Ni–Zr quaternary alloys calculated via a combined approach of geometric model and Miedema theory. Journal of Alloys and Compounds, 2006, 420, 175-181.	2.8	39
93	Thermodynamic description of the Al–Fe–Ni system over the whole composition and temperature ranges: Modeling coupled with key experiment. Calphad: Computer Coupling of Phase Diagrams and Thermochemistry, 2007, 31, 529-540.	0.7	39
94	Influence of Hf on the structure, thermal stability and oxidation resistance of Ti-Al-N coatings. Thin Solid Films, 2014, 565, 25-31.	0.8	39
95	Improving thermal stability of TiSiN nanocomposite coatings by multilayered epitaxial growth. Surface and Coatings Technology, 2017, 321, 180-185.	2.2	39
96	Insight into γ-Ni/γ′-Ni3Al interfacial energy affected by alloying elements. Materials and Design, 2017, 133, 39-46.	3.3	39
97	A Review of Calphad Modeling of Ordered Phases. Journal of Phase Equilibria and Diffusion, 2018, 39, 678-693.	0.5	39
98	Effect of Al content on microstructure and mechanical properties of Ti–Al–Si–N nanocomposite coatings. International Journal of Refractory Metals and Hard Materials, 2009, 27, 718-721.	1.7	38
99	Modeling of the viscosity in the AL–Cu–Mg–Si system: Database construction. Calphad: Computer Coupling of Phase Diagrams and Thermochemistry, 2015, 49, 79-86.	0.7	38
100	Microstructure and mechanical properties of gradient Ti(C, N) and TiN/Ti(C, N) multilayer PVD coatings. Materials Science & amp; Engineering A: Structural Materials: Properties, Microstructure and Processing, 2008, 478, 336-339.	2.6	37
101	CSUDDCC1—A diffusion database for multicomponent cemented carbides. International Journal of Refractory Metals and Hard Materials, 2014, 43, 164-180.	1.7	37
102	Interdiffusion in fcc Ni–X (XÂ=ÂRh, Ta, W, Re and Ir) alloys. Journal of Alloys and Compounds, 2016, 657, 457-463.	2.8	37
103	First-principles study of adsorption and diffusion of oxygen on surfaces of TiN, ZrN and HfN. Applied Surface Science, 2018, 452, 457-462.	3.1	37
104	Effects of F and Cl on the stability of MgH2. International Journal of Hydrogen Energy, 2014, 39, 877-883.	3.8	36
105	A first-principles study of structure, elasticity and thermal decomposition of Ti1â^'xTMxN alloys (TM=Y,) Tj ETQq1	10,7843 2,2	314 rgBT /Ov
106	Microstructure evolution of WC grains in WC–Co–Ni–Al alloys: Effect of binder phase composition. Journal of Alloys and Compounds, 2017, 710, 338-348.	2.8	36
107	Thermodynamic evaluation of the ZrO2î—,CeO2 system. Scripta Metallurgica Et Materialia, 1994, 31, 327-332.	1.0	35
108	Experimental investigation and thermodynamic modeling of the Cr-Ni-Si system. Metallurgical and Materials Transactions A: Physical Metallurgy and Materials Science, 2000, 31, 1795-1803.	1.1	35

#	Article	IF	CITATIONS
109	First-principles calculations of the thermodynamic and elastic properties of the L1 ₂ -based Al ₃ RE (RE = Sc, Y, La–Lu). International Journal of Materials Research, 2008, 99, 582-588.	0.1	35
110	A comparative research on magnetron sputtering and arc evaporation deposition of Ti–Al–N coatings. Thin Solid Films, 2011, 519, 3762-3767.	0.8	35
111	Thermodynamic description of the Al–Cu–Mg–Mn–Si quinary system and its application to solidification simulation. Thermochimica Acta, 2011, 512, 258-267.	1.2	35
112	First-principles study of the critical thickness in asymmetric ferroelectric tunnel junctions. Applied Physics Letters, 2011, 98, .	1.5	35
113	Effect of temperature gradient on microstructure evolution in Ni–Al–Cr bond coat/substrate systems: A phase-field study. Surface and Coatings Technology, 2015, 261, 364-374.	2.2	35
114	Texture, Microstructure and Mechanical Properties of 6111 Aluminum Alloy Subject to Rolling Deformation. Materials Research, 2017, 20, 1360-1368.	0.6	35
115	A predictive equation for solute diffusivity in liquid metals. Scripta Materialia, 2006, 55, 367-370.	2.6	34
116	On the reaction scheme and liquidus surface in the ternary system Al–Si–Ti. International Journal of Materials Research, 2008, 99, 705-711.	0.1	34
117	Effects of Cu content on the precipitation process of Al–Zn–Mg alloys. Journal of Materials Science, 2012, 47, 8174-8187.	1.7	34
118	Thermal stability and oxidation resistance of Cr1â^'xAlxN coatings with single phase cubic structure. Journal of Vacuum Science and Technology A: Vacuum, Surfaces and Films, 2015, 33, .	0.9	34
119	Structural, mechanical and thermal properties of CrAlNbN coatings. Surface and Coatings Technology, 2018, 349, 894-900.	2.2	34
120	Phase equilibria of the Cu–Ni–Si system at 700°C. Journal of Alloys and Compounds, 2011, 509, 9776-9781.	. 2.8	33
121	Density-functional theory study of Aln and Alnâ^'1Mg (n=2–17) clusters. Computational and Theoretical Chemistry, 2012, 984, 68-75.	1.1	33
122	Influence of Zr on structure, mechanical and thermal properties of Cr–Al–N coatings. Surface and Coatings Technology, 2015, 275, 289-295.	2.2	33
123	Thermodynamic database of multi-component Mg alloys and its application to solidification and heat treatment. Journal of Magnesium and Alloys, 2016, 4, 249-264.	5.5	33
124	Phase equilibria, thermodynamics and microstructure simulation of metastable spinodal decomposition in c–Ti1â^'xAlxN coatings. Calphad: Computer Coupling of Phase Diagrams and Thermochemistry, 2017, 56, 92-101.	0.7	33
125	Thermodynamic properties of the Al–Nb–Ni system. Intermetallics, 2003, 11, 995-1013.	1.8	32
126	Thermodynamic description of the Al–Fe–Mg–Mn–Si system and investigation of microstructure and microsegregation during directional solidification of an Al–Fe–Mg–Mn–Si alloy. International Journal of Materials Research, 2005, 96, 1351-1362.	0.8	32

#	Article	IF	CITATIONS
127	Experimental identification of the degenerated equilibrium and thermodynamic modeling in the Al–Nb system. Journal of Alloys and Compounds, 2008, 460, 632-638.	2.8	32
128	Recent progress in criterions for glass forming ability. Transactions of Nonferrous Metals Society of China, 2009, 19, 78-84.	1.7	32
129	Improved properties of Ti-Al-N coating by multilayer structure. International Journal of Refractory Metals and Hard Materials, 2011, 29, 681-685.	1.7	32
130	A new approach to control the segregation of (Ta,W)C cubic phase in ultrafine WC–10Co–0.5Ta cemented carbides. Scripta Materialia, 2015, 100, 48-50.	2.6	32
131	Thermal conductivity of the Mg–Al–Zn alloys: Experimental measurement and CALPHAD modeling. Calphad: Computer Coupling of Phase Diagrams and Thermochemistry, 2018, 62, 99-108.	0.7	32
132	Thermodynamic reassessment of the Al – V system. International Journal of Materials Research, 2004, 95, 978-986.	0.8	31
133	Phase equilibria of the system. Calphad: Computer Coupling of Phase Diagrams and Thermochemistry, 2009, 33, 624-627.	0.7	31
134	Thermodynamic and physical properties of FeAl and Fe3Al: an atomistic study by EAM simulation. Physica B: Condensed Matter, 2012, 407, 4530-4536.	1.3	31
135	On the scaling factor in Debye–Grüneisen model: A case study of the Mg–Zn binary system. Computational Materials Science, 2015, 98, 34-41.	1.4	31
136	Experimental investigation of the Nb-Ni phase diagram. Journal of Materials Science, 2005, 40, 6019-6022.	1.7	30
137	On the melting of Cr5Si3 and update of the thermodynamic description of Cr–Si. Calphad: Computer Coupling of Phase Diagrams and Thermochemistry, 2009, 33, 211-214.	0.7	30
138	High-throughput determination of the composition-dependent interdiffusivities in Cu-rich fcc Cu–Ag–Sn alloys at 1073 K. Journal of Alloys and Compounds, 2015, 644, 687-693.	2.8	30
139	Experimental Investigation and Thermodynamic Description of the Constitution of the Ternary System Crâ€si . Journal of the American Ceramic Society, 2000, 83, 2067-2073.	1.9	29
140	Experimental investigation and thermodynamic assessment of the C–Co–Fe–Ni–W system. International Journal of Refractory Metals and Hard Materials, 2016, 54, 60-69.	1.7	29
141	Interdiffusion between gadolinia doped ceria and yttria stabilized zirconia in solid oxide fuel cells: Experimental investigation and kinetic modeling. Journal of Power Sources, 2019, 441, 227152.	4.0	29
142	Phase equilibria of the Co–Ni–Ta system at 1100°C. Journal of Alloys and Compounds, 2006, 425, 153-158.	2.8	28
143	Experimental investigation and thermodynamic modeling of the Cu–Mn–Ni system. Calphad: Computer Coupling of Phase Diagrams and Thermochemistry, 2009, 33, 642-649.	0.7	28
144	Thermodynamic reassessment of the Al–Cr–Si system with the refined description of the Al–Cr system. Thermochimica Acta, 2013, 561, 77-90.	1.2	28

#	Article	IF	CITATIONS
145	Update of Al-Fe-Si, Al-Mn-Si and Al-Fe-Mn-Si thermodynamic descriptions. Transactions of Nonferrous Metals Society of China, 2014, 24, 2041-2053.	1.7	28
146	High-throughput measurement of the composition-dependent interdiffusivity matrices in Ni-rich fcc Ni-Al-Ta alloys at elevated temperatures. Journal of Alloys and Compounds, 2016, 688, 320-328.	2.8	28
147	Experimental investigation and thermodynamic description of the Cu-Cr-Zr system. Calphad: Computer Coupling of Phase Diagrams and Thermochemistry, 2017, 59, 1-11.	0.7	28
148	Simultaneously enhanced strength and ductility of 6xxx Al alloys via manipulating meso-scale and nano-scale structures guided with phase equilibrium. Journal of Materials Science and Technology, 2020, 41, 139-148.	5.6	28
149	Thermodynamic Assessment of the Zirconia-Urania System. Journal of the American Ceramic Society, 1996, 79, 521-524.	1.9	27
150	A thermodynamic description of the B–Co system: modeling and experiment. International Journal of Materials Research, 2002, 93, 1157-1163.	0.8	27
151	Thermodynamic modeling of the Cu–Mn system supported by key experiments. Journal of Alloys and Compounds, 2008, 457, 233-238.	2.8	27
152	Atomic mobilities and diffusivities in Al alloys. Science China Technological Sciences, 2012, 55, 306-328.	2.0	27
153	A pyridine vapor sensor based on metal-organic framework-modified quartz crystal microbalance. Sensors and Actuators B: Chemical, 2018, 254, 872-877.	4.0	27
154	Phase field simulation of the phase separation in the TiC-ZrC-WC system. Calphad: Computer Coupling of Phase Diagrams and Thermochemistry, 2018, 63, 190-195.	0.7	27
155	Thermodynamic modeling of YO1.5-TaO2.5 system and the effects of elastic strain energy and diffusion on phase transformation of YTaO4. Journal of the European Ceramic Society, 2019, 39, 5036-5047.	2.8	27
156	A novel approach to calculate diffusion matrix in ternary systems: Application to Ag–Mg–Mn and Cu–Ni–Sn systems. Calphad: Computer Coupling of Phase Diagrams and Thermochemistry, 2020, 68, 101708.	0.7	27
157	Thermodynamic description of the system Ti-Cr-C. Calphad: Computer Coupling of Phase Diagrams and Thermochemistry, 1999, 23, 393-408.	0.7	26
158	Structure and thermodynamics of the key precipitated phases in the Al–Mg–Si alloys from first-principles calculations. Journal of Materials Science, 2011, 46, 7839-7849.	1.7	26
159	Effects of pressure and vibration on the thermal decomposition of cubic Ti1-x Al x N, Ti1-x Zr x N, and Zr1-x Al x N coatings: a first-principles study. Journal of Materials Science, 2012, 47, 7621-7627.	1.7	26
160	Development of an atomic mobility database for disordered and ordered fcc phases in multicomponent Al alloys: focusing on binary systems. International Journal of Materials Research, 2013, 104, 135-148.	0.1	26
161	Thermodynamic calculation of the ZrO2-YO1.5-CaO phase diagram. Calphad: Computer Coupling of Phase Diagrams and Thermochemistry, 1992, 16, 355-362.	0.7	25
162	Structure, elastic and thermodynamic properties of the Ni–P system from first-principles calculations. Calphad: Computer Coupling of Phase Diagrams and Thermochemistry, 2011, 35, 284-291.	0.7	25

#	Article	IF	CITATIONS
163	Thermodynamic modeling of fcc order/disorder transformations in the Co–Pt system. Calphad: Computer Coupling of Phase Diagrams and Thermochemistry, 2011, 35, 323-330.	0.7	25
164	Effect of Zr on structure and properties of Ti–Al–N coatings with varied bias. International Journal of Refractory Metals and Hard Materials, 2013, 38, 81-86.	1.7	25
165	Interdiffusion and atomic mobility studies in Ni-rich fcc Niâ^'Alâ^'Mn alloys. Journal of Alloys and Compounds, 2013, 579, 124-131.	2.8	25
166	Phase equilibria in the Al–C–Ni–W quaternary system. International Journal of Refractory Metals and Hard Materials, 2014, 46, 43-51.	1.7	25
167	Phase-Field Simulation of Microstructure Evolution in Industrial A2214 Alloy During Solidification. Metallurgical and Materials Transactions A: Physical Metallurgy and Materials Science, 2015, 46, 3182-3191.	1.1	25
168	Microstructure and composition of segregation layers at WC/Co interfaces in ultrafine-grained cemented carbides co-doped with Cr and V. International Journal of Refractory Metals and Hard Materials, 2016, 58, 68-73.	1.7	25
169	A thermodynamic description of the Al–Co–Ni system and site occupancy in CoÂ+ÂAlNi3 composite binder phase. Journal of Alloys and Compounds, 2016, 687, 855-866.	2.8	25
170	Effect of V-addition on the thermal stability and oxidation resistance of CrAlN coatings. Ceramics International, 2018, 44, 7013-7019.	2.3	25
171	A MGI-oriented investigation of the Young's modulus and its application to the development of a novel Ti–Nb–Zr–Cr bio-alloy. Materials Science and Engineering C, 2020, 106, 110265.	3.8	25
172	Isothermal section at 1000°C of the Nb–Ti–Si system. Journal of Alloys and Compounds, 2005, 394, 235-239.	2.8	24
173	Reassessment of the Ce–Ni binary system supported by key experiments and ab initio calculations. Intermetallics, 2007, 15, 1401-1408.	1.8	24
174	Mobilities and diffusivities in fcc Co–X (X=Ag, Au, Cu, Pd and Pt) alloys. Calphad: Computer Coupling of Phase Diagrams and Thermochemistry, 2009, 33, 695-703.	0.7	24
175	Correlation between thermodynamics and glass forming ability in the Al–Ce–Ni system. Intermetallics, 2010, 18, 900-906.	1.8	24
176	Entropy favored ordering: Phase stability of Ni3Pt revisited by first-principles. Intermetallics, 2010, 18, 961-964.	1.8	24
177	Structural, phonon and thermodynamic properties of fcc-based metal nitrides from first-principles calculations. Calphad: Computer Coupling of Phase Diagrams and Thermochemistry, 2012, 37, 126-131.	0.7	24
178	Ternary diffusion in Cu-rich fcc Cu–Al–Si alloys at 1073 K. Journal of Alloys and Compounds, 2013, 566, 156-163.	2.8	24
179	Experimental investigation and computational study of atomic mobility in fcc ternary Co–Cr–W alloys. Calphad: Computer Coupling of Phase Diagrams and Thermochemistry, 2014, 45, 118-126.	0.7	24
180	Solubilities of grain-growth inhibitors in WC-Co-based cemented carbides: Thermodynamic calculations compared to experimental data. International Journal of Refractory Metals and Hard Materials, 2016, 61, 121-127.	1.7	24

#	Article	IF	CITATIONS
181	Effects of the volume changes and elastic-strain energies on the phase transition in the Li-Sn battery. Journal of Power Sources, 2016, 330, 111-119.	4.0	24
182	Ternary Co–Ni–B amorphous alloy with a superior electrochemical performance in a wide temperature range. International Journal of Hydrogen Energy, 2016, 41, 3955-3960.	3.8	24
183	C15 NbCr2 Laves phase with mechanical properties beyond Pugh's criterion. Computational Materials Science, 2016, 121, 167-173.	1.4	24
184	Investigation of diffusion behavior and mechanical properties of Mg-Zn system. Calphad: Computer Coupling of Phase Diagrams and Thermochemistry, 2019, 65, 204-211.	0.7	24
185	Preparation of millimeter scale second phase particles in aluminum alloys and determination of their mechanical properties. Journal of Alloys and Compounds, 2019, 784, 68-75.	2.8	24
186	Sintering behavior and mechanical properties of Cr3C2 doped ultra-fine WC-Co cemented carbides: Experment guided with thermodynamic calculations. International Journal of Refractory Metals and Hard Materials, 2019, 78, 240-246.	1.7	24
187	An investigation on the thermodynamic stability of V6Si5. Journal of Materials Science, 2007, 42, 7046-7048.	1.7	23
188	First-principles calculations of mechanical and thermodynamic properties of the Laves C15-Mg2RE (RE=La, Ce, Pr, Nd, Pm, Sm, Gd). Computational Materials Science, 2009, 47, 297-301.	1.4	23
189	Experimental investigation and thermodynamic calculation of the Fe–Mg–Mn and Fe–Mg–Ni systems. International Journal of Materials Research, 2011, 102, 6-16.	0.1	23
190	A new approach to establish both stable and metastable phase equilibria for fcc ordered/disordered phase transition: application to the Al–Ni and Ni–Si systems. Materials Chemistry and Physics, 2012, 135, 94-105.	2.0	23
191	Thermodynamic evaluation of the C–Ta–Ti system and extrapolation to the C–Ta–Ti–N system. International Journal of Refractory Metals and Hard Materials, 2013, 40, 36-42.	1.7	23
192	Experimental Investigation and Computer Simulation of Gradient Zone Formation in WC-Ti(C,N)-TaC-NbC-Co Cemented Carbides. Journal of Phase Equilibria and Diffusion, 2013, 34, 202-210.	0.5	23
193	Diffusional behaviors and mechanical properties of Cu–Zn system. Journal of Alloys and Compounds, 2020, 812, 152141.	2.8	23
194	The phase equilibria of the Cu–Cr–Ni and Cu–Cr–Ag systems: Experimental investigation and thermodynamic modeling. Calphad: Computer Coupling of Phase Diagrams and Thermochemistry, 2020, 68, 101734.	0.7	23
195	Atomic mobilities, zero-flux planes and flux reversals in fcc Cu–Fe–Ni alloys. Calphad: Computer Coupling of Phase Diagrams and Thermochemistry, 2011, 35, 376-383.	0.7	22
196	Experimental investigation and simulation of the effect of Ti and N contents on the formation of fcc-free surface layers in WC–Ti(C,N)–Co cemented carbides. International Journal of Refractory Metals and Hard Materials, 2013, 41, 638-647.	1.7	22
197	Diffusivities in liquid and fcc Al–Mg–Si alloys and their application to the simulation of solidification and dissolution processes. Calphad: Computer Coupling of Phase Diagrams and Thermochemistry, 2015, 49, 58-66.	0.7	22
198	Grain growth and hardness of TiC-based cermets: Experimental investigation and thermodynamic calculations. Ceramics International, 2016, 42, 19289-19295.	2.3	22

#	Article	IF	CITATIONS
199	Diffusion study in bcc_A2 Fe-Mn-Si system: Experimental measurement and CALPHAD assessment. Calphad: Computer Coupling of Phase Diagrams and Thermochemistry, 2017, 56, 230-240.	0.7	22
200	Structure, mechanical properties and thermal stability of Ti1-xSixN coatings. Ceramics International, 2018, 44, 15503-15508.	2.3	22
201	Thermodynamic calculation of the T0 curve and metastable phase diagrams of the Ti–M (M = Mo, V, Nb,) Tj ET 75-82.	Qq1 1 0.7 0.7	84314 rgBT 22
202	A thermodynamic modeling of the Cr–Nb–Ni system. Calphad: Computer Coupling of Phase Diagrams and Thermochemistry, 2005, 29, 140-148.	0.7	21
203	Construction of the Al–Ni–Si phase diagram over the whole composition and temperature ranges: thermodynamic modeling supported by key experiments and first-principles calculations. International Journal of Materials Research, 2008, 99, 598-612.	0.1	21
204	Study of atomic mobilities and diffusion characteristics in bcc Ti–Ta and Ta–W alloys. Calphad: Computer Coupling of Phase Diagrams and Thermochemistry, 2010, 34, 310-316.	0.7	21
205	Ab initio study of AlCu2M (M=Sc, Ti and Cr) ternary compounds under pressures. Computational Materials Science, 2011, 50, 2930-2937.	1.4	21
206	Phase change materials in the ternary system NH4Cl+CaCl2+H2O. Calphad: Computer Coupling of Phase Diagrams and Thermochemistry, 2011, 35, 269-275.	0.7	21
207	A thermodynamic description of the Co3Cr3Ti ternary system over the entire composition and temperature range. Calphad: Computer Coupling of Phase Diagrams and Thermochemistry, 2013, 41, 42-49.	0.7	21
208	Design of the Precipitation Process for Ni-Al Alloys with Optimal Mechanical Properties: A Phase-Field Study. Metallurgical and Materials Transactions A: Physical Metallurgy and Materials Science, 2014, 45, 1787-1802.	1.1	21
209	Microstructure and Thermal Conductivity of the As-Cast and Annealed Al–Cu–Mg–Si Alloys in the Temperature Range from \$\$25,^{circ }hbox {C}\$\$ 25 â~ C to \$\$400,^{circ }hbox {C}\$\$ 400 â~ C. International Journal of Thermophysics, 2015, 36, 2869-2880.	1.0	21
210	A thermodynamic description of the C–Hf–Ta system over the whole composition and temperature ranges. Calphad: Computer Coupling of Phase Diagrams and Thermochemistry, 2016, 53, 1-9.	0.7	21
211	Thermodynamic reassessment of the Ni–Si–Ti system using a four-sublattice model for ordered/disordered fcc phases supported by first-principles calculations. Journal of Alloys and Compounds, 2017, 693, 344-356.	2.8	21
212	Enhanced hardness and age-hardening of TiAlN coatings through Ru-addition. Scripta Materialia, 2019, 162, 382-386.	2.6	21
213	Impact of V, Hf and Si on oxidation processes in Ti–Al–N: Insights from ab initio molecular dynamics. Surface and Coatings Technology, 2020, 381, 125125.	2.2	21
214	Design of novel NiSiAlY alloys in marine salt-spray environment: Part II. Al-Ni-Si-Y thermodynamic dataset. Journal of Materials Science and Technology, 2021, 89, 186-198.	5.6	21
215	Catalytic Hydrogen Evolution of NaBH4 Hydrolysis by Cobalt Nanoparticles Supported on Bagasse-Derived Porous Carbon. Nanomaterials, 2021, 11, 3259.	1.9	21
216	Thermodynamic Calculation of the ZrO2-YO1.5-MgO System. Journal of the American Ceramic Society, 1991, 74, 2107-2112.	1.9	20

#	Article	IF	CITATIONS
217	Thermodynamic modeling of the Al–Sr system. Journal of Alloys and Compounds, 2003, 358, 288-293.	2.8	20
218	Thermodynamic description of the Ni–Si–Ti ternary system. International Journal of Materials Research, 2006, 97, 543-555.	0.1	20
219	Experimental study and thermodynamic modelling of the ZrO2–LaO1.5 system. Calphad: Computer Coupling of Phase Diagrams and Thermochemistry, 2008, 32, 111-120.	0.7	20
220	Experimental Investigation and Thermodynamic Reassessment of the Cu-Fe-Si System. Metallurgical and Materials Transactions A: Physical Metallurgy and Materials Science, 2009, 40, 1811-1825.	1.1	20
221	Mobilities and diffusivities in fcc Fe–X (, Au, Cu, Pd and Pt) alloys. Calphad: Computer Coupling of Phase Diagrams and Thermochemistry, 2010, 34, 253-262.	0.7	20
222	Experimental investigation and thermodynamic modeling of the Mn–Ni–Si system. Calphad: Computer Coupling of Phase Diagrams and Thermochemistry, 2011, 35, 346-354.	0.7	20
223	Thermodynamic optimization of the Li–Mg and Al–Li–Mg systems. Calphad: Computer Coupling of Phase Diagrams and Thermochemistry, 2011, 35, 523-532.	0.7	20
224	Thermodynamic optimization of the Cu–Nd system. Journal of Alloys and Compounds, 2011, 509, 2679-2683.	2.8	20
225	Thermodynamic modeling of the Ge–Ti system supported by key experiment. Thermochimica Acta, 2011, 521, 148-154.	1.2	20
226	Diffusivities and atomic mobilities in fcc_A1 Ni–X (X=Ge, Ti and V) alloys. Calphad: Computer Coupling of Phase Diagrams and Thermochemistry, 2013, 41, 108-118.	0.7	20
227	Diffusion-controlled growth of fcc-free surface layers on cemented carbides: Experimental measurements coupled with computer simulation. International Journal of Refractory Metals and Hard Materials, 2013, 41, 531-539.	1.7	20
228	Thermodynamic modeling of the Cr–Ni–Ti system using a four-sublattice model for ordered/disordered bcc phases. Thermochimica Acta, 2014, 578, 35-42.	1.2	20
229	Influence of ZrN on oxidation resistance of Ti–Al–N coating. Surface and Coatings Technology, 2014, 244, 87-91.	2.2	20
230	Experimental investigation of phase equilibria in the Co–Hf system. Journal of Alloys and Compounds, 2015, 627, 251-260.	2.8	20
231	High-Throughput Description of Infinite Composition–Structure–Property–Performance Relationships of Lithium–Manganese Oxide Spinel Cathodes. Chemistry of Materials, 2018, 30, 2287-2298.	3.2	20
232	Structural evolution of oxygen on the surface of TiAlN: Ab initio molecular dynamics simulations. Applied Surface Science, 2019, 470, 520-525.	3.1	20
233	Experimental investigation and thermodynamic description of the Cr-Si-Ti system. Scandinavian Journal of Metallurgy, 2002, 31, 25-33.	0.3	19
234	Amorphous and nanocrystalline Al82Ni10Y8 alloy powder prepared by gas atomization. Intermetallics, 2005, 13, 393-398.	1.8	19

#	Article	IF	CITATIONS
235	DETERMINATION OF PHASE DIAGRAMS USING EQUILIBRATED ALLOYS. , 2007, , 108-150.		19
236	Assessment of the atomic mobility in fcc Al–Cu–Mg alloys. Calphad: Computer Coupling of Phase Diagrams and Thermochemistry, 2010, 34, 286-293.	0.7	19
237	Effects of synthesis conditions on layered Li[Ni1/3Co1/3Mn1/3]O2 positive-electrode via hydroxide co-precipitation method for lithium-ion batteries. Transactions of Nonferrous Metals Society of China, 2011, 21, 114-120.	1.7	19
238	Native defects in LiNH <mml:math <br="" xmlns:mml="http://www.w3.org/1998/Math/MathML">display="inline"><mml:mrow><mml:msub><mml:mrow /><mml:mrow><mml:mn>2</mml:mn></mml:mrow></mml:mrow </mml:msub></mml:mrow></mml:math> : A first-principles study. Physical Review B, 2011, 84, .	1.1	19
239	Diffusion characteristics and atomic mobilities for bcc refractory Mo–Ta, Mo–W, and Mo–Nb alloys. Calphad: Computer Coupling of Phase Diagrams and Thermochemistry, 2012, 36, 110-117.	0.7	19
240	Development of an atomic mobility database for liquid phase in multicomponent Al alloys: focusing on binary systems. International Journal of Materials Research, 2013, 104, 721-735.	0.1	19
241	Thermodynamic description, diffusivities and atomic mobilities in binary Ni–Os system. Calphad: Computer Coupling of Phase Diagrams and Thermochemistry, 2015, 50, 118-125.	0.7	19
242	Influence of Ti on the mechanical properties, thermal stability and oxidation resistance of Al–Cr–N coatings. Vacuum, 2015, 120, 127-131.	1.6	19
243	Ab initio molecular dynamics studies on effect of Zr on oxidation resistance of TiAlN coatings. Applied Surface Science, 2016, 378, 293-300.	3.1	19
244	Morphologies of Primary Silicon in Hypereutectic Al-Si Alloys: Phase-Field Simulation Supported by Key Experiments. Metallurgical and Materials Transactions A: Physical Metallurgy and Materials Science, 2016, 47, 1510-1516.	1.1	19
245	A Novel Thermodynamic Model for Obtaining Solid–Liquid Interfacial Energies. Metallurgical and Materials Transactions A: Physical Metallurgy and Materials Science, 2017, 48, 5766-5770.	1.1	19
246	Interdiffusion behaviors and mechanical properties of Cu-Zr system. Calphad: Computer Coupling of Phase Diagrams and Thermochemistry, 2018, 61, 92-97.	0.7	19
247	Thermodynamic investigation of the Ag–Bi–Sn ternary system. Calphad: Computer Coupling of Phase Diagrams and Thermochemistry, 2008, 32, 152-163.	0.7	18
248	Phase equilibria and thermal analysis in the Fe–Mn–Ni system. International Journal of Materials Research, 2009, 100, 160-175.	0.1	18
249	Reaction Scheme and Liquidus Surface of the Ternary System Aluminum-Chromium-Titanium. Metallurgical and Materials Transactions A: Physical Metallurgy and Materials Science, 2009, 40, 2980-2986.	1.1	18
250	Heat capacities of several Al–Ni–Ti compounds. Thermochimica Acta, 2009, 486, 57-65.	1.2	18
251	Ferromagnetic ordering and mobility end-members for impurity diffusion in bcc Fe. Calphad: Computer Coupling of Phase Diagrams and Thermochemistry, 2009, 33, 732-736.	0.7	18
252	The effect of Ti atom on hydrogenation of Al(111) surface: First-principles studies. International Journal of Hydrogen Energy, 2010, 35, 609-613.	3.8	18

#	Article	IF	CITATIONS
253	Experimental investigation and thermodynamic reassessment of the Fe–Si–Zn system. Calphad: Computer Coupling of Phase Diagrams and Thermochemistry, 2010, 34, 405-414.	0.7	18
254	Thermodynamic modeling of the C–RE (RE=La, Ce and Pr) systems. Calphad: Computer Coupling of Phase Diagrams and Thermochemistry, 2011, 35, 533-541.	0.7	18
255	The structural stability, elastic constants and electronic structure of Al–Sr intermetallics by first-principles calculations. Physica B: Condensed Matter, 2011, 406, 3681-3686.	1.3	18
256	Microstructure and composition of the grain/binder interface in WC–Ni3Al composites. International Journal of Refractory Metals and Hard Materials, 2014, 44, 88-93.	1.7	18
257	Phase equilibria of the Mg–Mn–Zn system at 593ÂK (320°C). Journal of Alloys and Compounds, 2016, 688, 1115-1124.	' 2 . 8	18
258	A thermodynamic evaluation of the C–Cr–Nb system. Calphad: Computer Coupling of Phase Diagrams and Thermochemistry, 2016, 53, 10-19.	0.7	18
259	High-throughput measurements of interdiffusivity matrices in face centered cubic Ni–Al–Mo alloys at 1273–1473 K. Journal of Materials Research, 2017, 32, 2188-2201.	1.2	18
260	Thermophysical Properties: Key Input for ICME and MG. Journal of Phase Equilibria and Diffusion, 2017, 38, 601-602.	0.5	18
261	On the atomic model of Guinier-Preston zones in Al-Mg-Si-Cu alloys. Journal of Alloys and Compounds, 2018, 745, 644-650.	2.8	18
262	An in-situ study on the diffusion growth of intermetallic compounds in the Al–Mg diffusion couple. Journal of Alloys and Compounds, 2019, 810, 151878.	2.8	18
263	Mechanical properties and oxidation resistance of chemically vapor deposited TiSiN nanocomposite coating with thermodynamically designed compositions. International Journal of Refractory Metals and Hard Materials, 2019, 80, 30-39.	1.7	18
264	Mechanical properties and microstructures of Al-10Mg-4.5Si matrix composites reinforced by carbon nanotubes. Journal of Alloys and Compounds, 2019, 792, 860-868.	2.8	18
265	Effect of Manganese on Microstructure and Corrosion Behavior of the Mg-3Al Alloys. Metals, 2019, 9, 460.	1.0	18
266	<mml:math <br="" xmlns:mml="http://www.w3.org/1998/Math/MathML">altimg="si2.svg"><mml:msup><mml:mrow><mml:mi>β</mml:mi></mml:mrow><mml:mrow><mml:mtext>'needle-shape precipitate formation in Al-Mg-Si alloy: Phase field simulation and experimental verification. Computational Materials Science, 2020, 184, 109878.</mml:mtext></mml:mrow></mml:msup></mml:math>	l:mtext>< 1.4	mml:mtext:
267	Effect of melt holding on morphological evolution and sedimentation behavior of iron-rich intermetallic phases in Al—Si—Fe—Mn—Mg alloy. Transactions of Nonferrous Metals Society of China, 2020, 30, 1-13.	1.7	18
268	The crystal structure of a new triclinic ternary phase: τ3-Cr4(Al, Si)11. Intermetallics, 2006, 14, 224-226.	1.8	17
269	First-principles study of binary special quasirandom structures for the Al–Cu, Al–Si, Cu–Si, and Mg–Si systems. Calphad: Computer Coupling of Phase Diagrams and Thermochemistry, 2009, 33, 769-773.	0.7	17
270	The phase equilibria of the Al–Ce–Ni system at 500°C. Journal of Alloys and Compounds, 2009, 470, 222-227.	2.8	17

#	Article	IF	CITATIONS
271	Thermodynamic investigation of the galvanizing systems, II: Thermodynamic evaluation of the Ni–Zn system. Calphad: Computer Coupling of Phase Diagrams and Thermochemistry, 2011, 35, 276-283.	0.7	17
272	Simulation of the electron diffraction patterns from needle/rod-like precipitates in Al–Mg–Si alloys. Materials Characterization, 2011, 62, 894-903.	1.9	17
273	First-principles study on the crystal, electronic structure and mechanical properties of hexagonal Al3RE (RE = La, Ce, Pr, Nd, Sm, Gd) intermetallic compounds. Solid State Communications, 2011, 151, 1135-1140.	0.9	17
274	First-principles investigations of elastic, electronic and thermodynamic properties of Al12X (XÂ=ÂMo, W) Tj ETQq	0 0 0 rgBT 1.8	⁻ /Overlock 1 17
275	Diffusivities and Atomic Mobilities of Sn-Bi and Sn-Pb Melts. Journal of Electronic Materials, 2013, 42, 1158-1170.	1.0	17
276	Integrating computational modeling and first-principles calculations to predict stacking fault energy of dilute multicomponent Ni-base alloys. Computational Materials Science, 2014, 91, 50-55.	1.4	17
277	Experiments and modeling of double-peak precipitation hardening and strengthening mechanisms in Al-Zn-Mg alloy. Transactions of Nonferrous Metals Society of China, 2014, 24, 2138-2144.	1.7	17
278	Thermodynamic assessment of the Co–Mo–Ni and Mo–Ni–W ternary systems. Calphad: Computer Coupling of Phase Diagrams and Thermochemistry, 2016, 55, 243-251.	0.7	17
	Diffusivities and atomic mobilities for fcc Cu–Ni–Sn alloys, Calphad: Computer Coupling of Phase		

279	Diagrams and Thermochemistry, 2017, 59, 84-89.	0.7	17
280	Atomic mobilities and diffusivities in fcc Co–X (X = Mn, Pt and Re) alloys. Calphad: Computer Coupling of Phase Diagrams and Thermochemistry, 2019, 64, 306-312.	0.7	17
281	Diffusivity and atomic mobility for fcc Ni–Cu–Ti alloy: Measurements and an intelligent modeling. Calphad: Computer Coupling of Phase Diagrams and Thermochemistry, 2020, 70, 101780.	0.7	17
282	Interface enhanced mechanical and thermal properties of TiSiN/TiAlN multilayers. Journal of Alloys and Compounds, 2021, 861, 158571.	2.8	17
283	Effect of bimodal WC particle size and binder composition on the morphology of WC grains in WC–Co–Ni3Al cemented carbides. Journal of Materials Research and Technology, 2021, 12, 1747-1754.	2.6	17
284	High-throughput determination of the composition-dependent mechanical and diffusion properties in β Ti–Nb–Zr–Hf refractory alloys. Journal of Alloys and Compounds, 2021, 876, 160150.	2.8	17
285	Densification, grain growth mechanism and mechanical properties of Mo 10Nb refractory targets fabricated by SPS. International Journal of Refractory Metals and Hard Materials, 2021, 99, 105575.	1.7	17
286	Experimental identification of the degenerated equilibrium in extreme Al end of the Al–Cr system. Journal of Materials Science, 2005, 40, 1023-1025.	1.7	16
287	Experimental investigation of the Al–Ce–Ni system at 800°C. Intermetallics, 2008, 16, 432-439.	1.8	16

Phase equilibria of the Fe–Ni–Si system at 850°C. Journal of Alloys and Compounds, 2009, 481, 509-514. 2.8 16

#	Article	IF	CITATIONS
289	A thermodynamic modeling of the C–Cr–Ta ternary system. Journal of Alloys and Compounds, 2011, 509, 5996-6003.	2.8	16
290	Effect of Al and Si additions on microstructure and mechanical properties of TiN coatings. Journal of Central South University, 2011, 18, 310-313.	1.2	16
291	Thermodynamic modeling of the C–W–Zr system. International Journal of Refractory Metals and Hard Materials, 2015, 50, 274-281.	1.7	16
292	A new type of double-layer gradient cemented carbides: Preparation and microstructure characterization. Scripta Materialia, 2016, 123, 73-76.	2.6	16
293	Experimental Investigation and Thermodynamic Description of the Cu-Zr System. Journal of Phase Equilibria and Diffusion, 2017, 38, 121-134.	0.5	16
294	Influence of deformation microstructure on the precipitation behaviors of an Al-4Mg-0.3Cu alloy. Journal of Alloys and Compounds, 2017, 695, 2238-2245.	2.8	16
295	Experimental investigation of the isothermal section of the Mg–Ni–Y system with LPSO phases at 400°C. Journal of Materials Science, 2018, 53, 9243-9257.	1.7	16
296	Microstructure, mechanical properties and cutting performances of TiSiCN super-hard nanocomposite coatings deposited using CVD method under the guidance of thermodynamic calculations. Surface and Coatings Technology, 2019, 378, 124956.	2.2	16
297	Influence of Cr3C2 and VC Content on WC Grain Size, WC Shape and Mechanical Properties of WC–6.0 wt. % Co Cemented Carbides. Materials, 2021, 14, 1551.	1.3	16
298	A new model for thermal conductivity of "continuous matrix / dispersed and separated 3D-particles― type composite materials and its application to WC-M (MÂ=ÂCo, Ag) systems. Journal of Materials Science and Technology, 2022, 97, 123-133.	5.6	16
299	Thermodynamic assessment of the ZrO2-LaO1.5 system. Journal of the European Ceramic Society, 1995, 15, 503-511.	2.8	15
300	Thermodynamic calculation of the Ndî—,Ni system. Calphad: Computer Coupling of Phase Diagrams and Thermochemistry, 1996, 20, 289-296.	0.7	15
301	An effective approach to describe growth of binary intermediate phases with narrow ranges of homogeneity. Metallurgical and Materials Transactions A: Physical Metallurgy and Materials Science, 2001, 32, 2396-2400.	1.1	15
302	Phase equilibria of the Fe–Nb–Ti system at 900°C. Journal of Alloys and Compounds, 2005, 396, 151-155.	2.8	15
303	First principle study of AlX (X=3d,4d,5d elements and Lu) dimer. Journal of Chemical Physics, 2008, 128, 074305.	1.2	15
304	Elastic and thermodynamic properties of the Ni–B system studied by first-principles calculations and experimental measurements. Calphad: Computer Coupling of Phase Diagrams and Thermochemistry, 2010, 34, 245-251.	0.7	15
305	Thermodynamic Modeling of the La-B and La-Bi Systems Supported by First-Principles Calculations. Journal of Phase Equilibria and Diffusion, 2013, 34, 297-306.	0.5	15
306	Modeling of the molar volume of the solution phases in the Al–Cu–Mg system. Calphad: Computer Coupling of Phase Diagrams and Thermochemistry, 2015, 51, 261-271.	0.7	15

#	Article	IF	CITATIONS
307	Phase-Field Model of Finite Interface Dissipation: A Novel Way to Directly Couple with CALPHAD Databases. Journal of Phase Equilibria and Diffusion, 2016, 37, 259-260.	0.5	15
308	CALPHAD-type thermodynamic assessment of the Ti–Mo–Cr–V quaternary system. Calphad: Computer Coupling of Phase Diagrams and Thermochemistry, 2016, 55, 103-112.	0.7	15
309	Reassessment of Atomic Mobilities in fcc Cu-Ag-Sn System Aiming at Establishment of an Atomic Mobility Database in Sn-Ag-Cu-In-Sb-Bi-Pb Solder Alloys. Journal of Electronic Materials, 2017, 46, 2119-2129.	1.0	15
310	Morphology of η phase in cemented carbides with Fe-based binders influenced by carbon content and nitrogen atmosphere. Ceramics International, 2019, 45, 20774-20779.	2.3	15
311	Development and application of phase diagrams for Li-ion batteries using CALPHAD approach. Progress in Natural Science: Materials International, 2019, 29, 265-276.	1.8	15
312	Structural, mechanical and thermal properties of Ti1-xSixN/CrAlN (xÂ=Â0, 0.13 and 0.22) multilayers. Journal of Alloys and Compounds, 2019, 800, 355-362.	2.8	15
313	Influence of Ru-addition on thermal decomposition and oxidation resistance of TiAlN coatings. Surface and Coatings Technology, 2020, 401, 126234.	2.2	15
314	Diffusion growth of Ï• ternary intermetallic compound in the Mg-Al-Zn alloy system: In-situ observation and modeling. Journal of Materials Science and Technology, 2021, 60, 222-229.	5.6	15
315	Investigation on the corrosion resistance of the Mg-10Al-xMn alloys based on thermodynamic calculations. Corrosion Science, 2021, 189, 109631.	3.0	15
316	Measurement and calculation of the ZrO2-CeO2-LaO1.5 phase diagram. Calphad: Computer Coupling of Phase Diagrams and Thermochemistry, 1996, 20, 95-108.	0.7	14
317	Nano-amorphous (FeAl)1â^'xZrx alloys prepared by mechanical alloying. Journal of Alloys and Compounds, 2006, 421, 314-318.	2.8	14
318	Experimental investigation on the phase equilibria of the Mn–Ni–Zn system at 400°C. Journal of Alloys and Compounds, 2010, 489, 362-368.	2.8	14
319	Experimental study of Al–Zr–Y system phase equilibria at 773K. Journal of Alloys and Compounds, 2010, 497, 118-120.	2.8	14
320	The phase relationships in the Al–Zr–Ho ternary system at 773K. Journal of Alloys and Compounds, 2010, 508, 79-84.	2.8	14
321	Heat capacities and thermodynamic properties of MgNDC. Journal of Thermal Analysis and Calorimetry, 2011, 103, 365-372.	2.0	14
322	Thermodynamic and mechanical stabilities of γ′-Ir3(Al,W). Journal of Applied Physics, 2011, 109, 023504.	1.1	14
323	Investigation of the as-solidified microstructure of an Al–Mg–Si–Cu alloy. Journal of Alloys and Compounds, 2014, 602, 312-321.	2.8	14
324	Simulation of atomic mobilities, diffusion coefficients and diffusion paths in bcc_A2 and bcc_B2 phases of the Al–Ni–Fe system. Journal of Alloys and Compounds, 2015, 634, 148-155.	2.8	14

#	Article	IF	CITATIONS
325	Experimental and thermodynamic investigation of gradient zone formation for Ti(C,N)-based cermets sintered in nitrogen atmosphere. Ceramics International, 2017, 43, 12089-12094.	2.3	14
326	Investigations on diffusion behaviors in Ti–rich Ti–Nb–Zr–Cr system: Experimental measurement and CALPHAD modeling. Calphad: Computer Coupling of Phase Diagrams and Thermochemistry, 2018, 62, 223-231.	0.7	14
327	A general model to calculate coherent solid/solid and immiscible liquid/liquid interfacial energies. Calphad: Computer Coupling of Phase Diagrams and Thermochemistry, 2019, 65, 225-231.	0.7	14
328	Experimental phase diagram, thermodynamic modeling and solidified microstructure in the Mo–Ni–W ternary system. Calphad: Computer Coupling of Phase Diagrams and Thermochemistry, 2020, 68, 101748.	0.7	14
329	The phase equilibria of the Ti–V–M (M = Si, Nb, Ta) ternary systems. Intermetallics, 2020, 118, 106701.	1.8	14
330	Self-accommodated defect structures modifying the growth of Laves phase. Journal of Materials Science and Technology, 2021, 62, 203-213.	5.6	14
331	Intrinsic Defects in LiMn ₂ O ₄ : First-Principles Calculations. ACS Omega, 2021, 6, 21255-21264.	1.6	14
332	Diffusional behaviors and mechanical properties of Ni-Zn system. Journal of Alloys and Compounds, 2021, 881, 160581.	2.8	14
333	First-principles investigation on stability and electronic structure of Sc-doped Î,′/Al interface in Alâ^'Cu alloys. Transactions of Nonferrous Metals Society of China, 2021, 31, 3342-3355.	1.7	14
334	Atomistic Observation of Temperature-Dependent Defect Evolution within Sub-stoichiometric WO _{3–<i>x</i>} Catalysts. ACS Applied Materials & Interfaces, 2022, 14, 2194-2201.	4.0	14
335	Phase equilibria of the Cu–Nb–Ti system at 850°C. Journal of Alloys and Compounds, 2005, 399, 92-95.	2.8	13
336	Isothermal section at 927 °C of Cr-Ni-Ti system. Transactions of Nonferrous Metals Society of China, 2007, 17, 711-714.	1.7	13
337	Phase equilibria of the Ni–Ti–Ta system at 927°C. Materials Science & Engineering A: Structural Materials: Properties, Microstructure and Processing, 2007, 448, 210-215.	2.6	13
338	Reaction Scheme and Liquidus Surface in the Al-Rich Section of the Al-Cr-Ni System. Metallurgical and Materials Transactions A: Physical Metallurgy and Materials Science, 2008, 39, 2363-2369.	1.1	13
339	First-principles calculations of elastic constants of DO ₃ -Mg ₃ RE (RE = Sc, Y, La,) Tj ETQ	q1 <u>1</u> 0.78 1.2	94314 rgBT /○
340	Heat capacities and thermodynamic properties of one manganese-based MOFs. Journal of Thermal Analysis and Calorimetry, 2010, 102, 1161-1166.	2.0	13
341	Thermodynamic assessment of the V–Zn system supported by key experiments and first-principles calculations. Calphad: Computer Coupling of Phase Diagrams and Thermochemistry, 2010, 34, 75-80.	0.7	13
342	Assessment of atomic mobilities in fcc Cu–Ni–Zn alloys. Calphad: Computer Coupling of Phase Diagrams and Thermochemistry, 2011, 35, 231-241.	0.7	13

#	Article	IF	CITATIONS
343	Phase Equilibria in the Ni-Sn-Zn System at 500°C. Journal of Electronic Materials, 2011, 40, 2290-2299.	1.0	13
344	Self-Diffusion Coefficient of fcc Mg: First-Principles Calculations and Semi-Empirical Predictions. Journal of Phase Equilibria and Diffusion, 2011, 32, 128-137.	0.5	13
345	Atomic mobilities, diffusivities and their kinetic implications for U– (, Nb and Mo) bcc alloys. Calphad: Computer Coupling of Phase Diagrams and Thermochemistry, 2012, 37, 49-56.	0.7	13
346	Effects of Zn impurities on the electronic properties of Pr doped CaTiO3. Physica B: Condensed Matter, 2012, 407, 849-854.	1.3	13
347	Phase stability, thermodynamic and mechanical properties of AlZr2, FeZr2 and Al2FeZr6 from first-principles calculations. Journal of Nuclear Materials, 2013, 440, 6-10.	1.3	13
348	The quaternary Al–Fe–Ni–Si phase equilibria in Al-rich corner: experimental measurement and thermodynamic modeling. Journal of Materials Science, 2014, 49, 1157-1169.	1.7	13
349	Experimental investigation and thermodynamic analysis of the Sc–Ni system supplemented with first-principles calculations. Thermochimica Acta, 2014, 586, 30-39.	1.2	13
350	Thermodynamic assessment of the C–Nb–Mo system over the entire composition and temperature ranges. Calphad: Computer Coupling of Phase Diagrams and Thermochemistry, 2015, 51, 104-110.	0.7	13
351	Predicting an alloying strategy for improving fracture toughness of C15 NbCr2 Laves phase: A first-principles study. Computational Materials Science, 2016, 123, 59-64.	1.4	13
352	Thermodynamic Modeling of the C-Co-Mo and C-Mo-Ni Ternary Systems. Journal of Phase Equilibria and Diffusion, 2016, 37, 423-437.	0.5	13
353	Phase equilibria and solidification characteristics of the Al–Sc–Si alloys. Journal of Materials Science, 2016, 51, 1644-1658.	1.7	13
354	Experimental Investigation of the Co-Ge Phase Diagram. Journal of Phase Equilibria and Diffusion, 2017, 38, 843-852.	0.5	13
355	Effects of Î,′ precipitates on the mechanical performance and fracture behavior of an Al–Cu alloy subjected to overaged condition. Materials Science & Engineering A: Structural Materials: Properties, Microstructure and Processing, 2019, 762, 138091.	2.6	13
356	Thermodynamic investigation of the Mg-Ni-Zn system by experiments and calculations and its application. Journal of Alloys and Compounds, 2019, 784, 769-787.	2.8	13
357	A general thermodynamic model for the long-period stacking ordered phases in magnesium alloys. Journal of Magnesium and Alloys, 2021, 9, 144-155.	5.5	13
358	Microstructure, mechanical and thermal properties of TiAlTaN/TiAlSiN multilayer. Vacuum, 2021, 187, 110138.	1.6	13
359	Effect of C content on the surface gradient structure of (Ti, Mo)(C, N) and Ti(C, N)-based cermets. Journal of Materials Research and Technology, 2022, 16, 544-554.	2.6	13
360	Developing Al–Fe–Si alloys with high thermal stability through tuning Fe, Si contents and cooling rates. Intermetallics, 2022, 144, 107505.	1.8	13

Үомс Du

#	Article	IF	CITATIONS
361	Thermodynamic description of the C-Fe-Mn system with key experiments and its practical applications. International Journal of Materials Research, 2008, 99, 1306-1318.	0.1	12
362	Phase Equilibria of the Mn-Si-Zn System at 600°C. Metallurgical and Materials Transactions A: Physical Metallurgy and Materials Science, 2009, 40, 2042-2047.	1.1	12
363	Effect of electron concentration on the Laves phase stability of NbCr ₂ –Ni produced by powder metallurgy. Philosophical Magazine Letters, 2009, 89, 465-473.	0.5	12
364	The Ternary System Nickel/Silicon/Titanium RevisitedÂÂ. Zeitschrift Fur Anorganische Und Allgemeine Chemie, 2010, 636, 982-990.	0.6	12
365	A thermodynamic reassessment of the Si–Sr system. Calphad: Computer Coupling of Phase Diagrams and Thermochemistry, 2011, 35, 594-600.	0.7	12
366	Large-scale synthesis of tungsten single-crystal microtubes via vapor-deposition process. Journal of Crystal Growth, 2011, 316, 137-144.	0.7	12
367	Correlation between arc evaporation of Ti–Al–N coatings and corresponding Ti0.50Al0.50 target types. Surface and Coatings Technology, 2015, 275, 309-315.	2.2	12
368	Interdiffusivities and atomic mobilities in FCC Co–Mo–W alloys. Calphad: Computer Coupling of Phase Diagrams and Thermochemistry, 2015, 49, 35-40.	0.7	12
369	Grain boundary diffusion and precipitates in B2 Tiâ~'50.2 at.% Ni alloy. Intermetallics, 2015, 61, 30-37.	1.8	12
370	Effect of the Cubic Phase Distribution on Ultrafine <scp>WC</scp> –10Co–0.5Cr– <i>x</i> Ta Cemented Carbide. Journal of the American Ceramic Society, 2016, 99, 1047-1054.	1.9	12
371	Microstructural Evolution and Structure-Hardness Relationship in an Al-4wt.%Mg Alloy Processed by High-Pressure Torsion. Journal of Materials Engineering and Performance, 2016, 25, 1909-1915.	1.2	12
372	First-principles prediction of structural, mechanical and magnetic properties in Ni2MnAl. Computational Materials Science, 2016, 123, 52-58.	1.4	12
373	Site preference and diffusion of hydrogen during hydrogenation of Mg: A first-principles study. International Journal of Hydrogen Energy, 2016, 41, 3508-3516.	3.8	12
374	Thermodynamic calculation designed compositions, microstructure and mechanical property of ultra-fine WC-10Co-Cr 3 C 2 -TaC cemented carbides. International Journal of Refractory Metals and Hard Materials, 2017, 69, 11-17.	1.7	12
375	Deposition of CVD-TiCN and TiAlN coatings guided with thermodynamic calculations. International Journal of Materials Research, 2018, 109, 277-283.	0.1	12
376	Atomic mobilities and diffusivities in U-X (X = Nb, Zr, Ti) bcc alloys. Calphad: Computer Coupling of Phase Diagrams and Thermochemistry, 2018, 61, 85-91.	0.7	12
377	Clarification of the Dissolution of Solid CaO and the Phosphorusâ€Enrichment Capability of Calcium Silicates in the Multiphase Slag Based on the Ion and Molecule Coexistence Theory. Steel Research International, 2018, 89, 1700317.	1.0	12
378	Influence of annealing on the microstructure and mechanical properties of MTCVD TiC0.79N0.21 coating. Vacuum, 2018, 148, 88-97.	1.6	12

#	Article	IF	CITATIONS
379	Transformation of fracture mode of an Al-Mg-Si-Cu alloy subject to aging treatment. Materials Science & Engineering A: Structural Materials: Properties, Microstructure and Processing, 2018, 735, 201-207.	2.6	12
380	A new model to describe composition and temperature dependence of thermal conductivity for solution phases in binary alloys. Journal of Materials Science and Technology, 2020, 59, 72-82.	5.6	12
381	Reaction layer formation at the interface between Ti or Zr and AlN. Physica Status Solidi A, 1996, 157, 99-106.	1.7	11
382	Experimental investigation and thermodynamic calculation in the Al-Be-Si ternary system. International Journal of Materials Research, 2005, 96, 1301-1307.	0.8	11
383	Determination of phase diagrams using the diffusion couple technique. Rare Metals, 2006, 25, 427-430.	3.6	11
384	Experimental study of the Be–Si phase diagram. Journal of Materials Science, 2006, 41, 2525-2528.	1.7	11
385	Thermodynamic reassessment of the Cu–Mg–Ni system with brief comments on the thermodynamic modeling of the sub-systems. Calphad: Computer Coupling of Phase Diagrams and Thermochemistry, 2008, 32, 675-685.	0.7	11
386	Measurement of the isothermal sections at 700 and 427 °C in the Al – Mg – Ni system. International Journal of Materials Research, 2008, 99, 907-911.	0.1	11
387	Phase equilibria of the Al–Ni–Zn system at 340°C. International Journal of Materials Research, 2008, 99, 644-649.	0.1	11
388	First-principles calculations of elastic and thermo-physical properties of Al, Mg and rare earth lanthanide elements. Physica B: Condensed Matter, 2009, 404, 2299-2304.	1.3	11
389	The isothermal section of the Gd–Ti–Si ternary system at 773 K. Journal of Alloys and Compounds, 2009, 475, 268-272.	2.8	11
390	Thermodynamic properties and heat capacities of Co (BTC)1/3 (DMF) (HCOO). Journal of Thermal Analysis and Calorimetry, 2010, 102, 1087-1093.	2.0	11
391	Spatial and electronic structure of the Ni3P surface. Applied Surface Science, 2010, 256, 7692-7695.	3.1	11
392	Phase equilibria in the Al–Zr–Ce system at 773K. Journal of Alloys and Compounds, 2010, 491, 200-202.	2.8	11
393	The isothermal section of the Ag–La–Sn ternary system at 400°C. Journal of Alloys and Compounds, 2010, 493, 122-127.	2.8	11
394	Assessment of atomic mobilities in fcc Al-Zn and Ni-Zn alloys. Calphad: Computer Coupling of Phase Diagrams and Thermochemistry, 2010, 34, 446-451.	0.7	11
395	Structural, electronic, elastic and thermodynamic properties of AlSi2RE (RE=La, Ce, Pr and Nd) from first-principle calculations. Computational Materials Science, 2011, 50, 3303-3310.	1.4	11
396	Experimental investigation and thermodynamic modeling of the Cu–Si–Zn system with the refined description for the Cu–Zn system. Calphad: Computer Coupling of Phase Diagrams and Thermochemistry, 2011, 35, 191-203.	0.7	11

#	Article	IF	CITATIONS
397	Exceptional thermal stability and thermodynamic properties of lithium based metal–organic framework. Journal of Thermal Analysis and Calorimetry, 2011, 103, 373-380.	2.0	11
398	Native defects and Pr impurities in orthorhombic CaTiO3 by first-principles calculations. Physica B: Condensed Matter, 2011, 406, 2697-2702.	1.3	11
399	Investigation of glass forming ability in Ce–Al–Ni alloys. Journal of Non-Crystalline Solids, 2012, 358, 1368-1373.	1.5	11
400	Thermodynamic modeling of the Ge–Sc system supported by key experiments and first-principles calculation. Calphad: Computer Coupling of Phase Diagrams and Thermochemistry, 2012, 37, 18-24.	0.7	11
401	Thermodynamic description of the Ge–Na and Ge–K systems using the CALPHAD approach supported by first-principles calculations. Calphad: Computer Coupling of Phase Diagrams and Thermochemistry, 2012, 37, 72-76.	0.7	11
402	Elastic, phonon and thermodynamic properties of Mg–Ga compounds from first-principles calculations. Calphad: Computer Coupling of Phase Diagrams and Thermochemistry, 2012, 37, 137-144.	0.7	11
403	Solid state phase equilibria and intermetallic compounds of the Al–Cr–Ho system. Journal of Solid State Chemistry, 2013, 198, 344-356.	1.4	11
404	A thermodynamic description of the C–Ta–Zr system. International Journal of Refractory Metals and Hard Materials, 2013, 41, 408-415.	1.7	11
405	Diffusivities and atomic mobilities of an Sn–Ag–Bi–Cu–Pb melt. International Journal of Materials Research, 2014, 105, 827-839.	0.1	11
406	Exploring phase stability, electronic and mechanical properties of Ce–Pb intermetallic compounds using first-principles calculations. Journal of Solid State Chemistry, 2016, 237, 385-393.	1.4	11
407	A Trial to Design γ∫γ′ Bond Coat in Ni–Al–Cr Mode TBCs Aided by Phase-Field Simulation. Coatings, 2018, 421.	⁸ 1.2	11
408	Thermodynamic modeling and solidified microstructure in the Mo–Nb–Zr ternary system. Calphad: Computer Coupling of Phase Diagrams and Thermochemistry, 2019, 66, 101630.	0.7	11
409	Modeling on the molar volume of the Al–Cu–Mg–Si system. Calphad: Computer Coupling of Phase Diagrams and Thermochemistry, 2020, 68, 101693.	0.7	11
410	Relation between the nitrogen gas pressure and structure characteristics of WC–Ti(C, N)–Co graded cemented carbides. Journal of Alloys and Compounds, 2020, 831, 154764.	2.8	11
411	Thermodynamic reassessment of the Mo–Hf and Mo–Zr systems supported by first-principles calculations. Calphad: Computer Coupling of Phase Diagrams and Thermochemistry, 2020, 69, 101766.	0.7	11
412	Structure and Mechanical Properties of PVD and CVD TiAlSiN Coatings Deposited on Cemented Carbide. Crystals, 2021, 11, 598.	1.0	11
413	Design of novel NiSiAlY alloys in marine salt-spray environment: Part I. Al-Si-Y and Ni-Si-Y subsystems. Journal of Materials Science and Technology, 2021, 88, 66-78.	5.6	11
414	Thermodynamic assessment of the Cu-Nd system. Scripta Materialia, 1996, 34, 1609-1613.	2.6	10

Үомс Du

#	Article	IF	CITATIONS
415	A Reinvestigation of the Constitution of the Partial System TiSi-Si. Journal of Materials Science Letters, 1998, 17, 1407-1408.	0.5	10
416	Isothermal section at 950°C of the Co–Nb–Ti system. Materials Science & Engineering A: Structural Materials: Properties, Microstructure and Processing, 2005, 412, 336-341.	2.6	10
417	Thermodynamic assessment of the Ce–Mn system. Journal of Alloys and Compounds, 2007, 437, 102-106.	2.8	10
418	(FeAl3)1â^²xZrx amorphous alloys prepared by mechanical alloying. Physica B: Condensed Matter, 2007, 391, 380-384.	1.3	10
419	Diffusion of hydrogen vacancy in Na3AlH6. Applied Physics Letters, 2009, 95, 111910.	1.5	10
420	Atomic mobilities and diffusion characteristics for fcc Cu–Ag–Au alloys. Calphad: Computer Coupling of Phase Diagrams and Thermochemistry, 2011, 35, 314-322.	0.7	10
421	Atomic mobility and diffusivity of bcc_A2 phase in the Fe–X (X=Cu,Si,Zn) systems. Calphad: Computer Coupling of Phase Diagrams and Thermochemistry, 2012, 36, 127-134.	0.7	10
422	Thermodynamic modeling of the Hf–Sn and Sn–Y systems. Calphad: Computer Coupling of Phase Diagrams and Thermochemistry, 2012, 39, 91-96.	0.7	10
423	Thermodynamic Modeling of the Li-H and Ca-H Systems. Journal of Phase Equilibria and Diffusion, 2012, 33, 89-96.	0.5	10
424	Diffusivities and Atomic Mobilities of Sn-Ag and Sn-In Melts. Journal of Electronic Materials, 2014, 43, 1131-1143.	1.0	10
425	Phase equilibria of the Mg–La–Nd system at 500°C. Journal of Alloys and Compounds, 2014, 585, 384-392.	2.8	10
426	Thermodynamic modeling of the Co–Hf system supported by key experiments and first-principles calculations. Thermochimica Acta, 2015, 608, 49-58.	1.2	10
427	An interatomic potential for simulation of defects and phase change of zirconium. Computational Materials Science, 2018, 147, 7-17.	1.4	10
428	Through-process modeling and experimental verification of titanium carbonitride coating prepared by moderate temperature chemical vapor deposition. Surface and Coatings Technology, 2019, 359, 278-288.	2.2	10
429	Effects of Cr3C2, VC, and TaC on Microstructure, WC Morphology and Mechanical Properties of Ultrafine WC–10 wt. % Co Cemented Carbides. Metals, 2020, 10, 1211.	1.0	10
430	Optimization of the mechanical properties of ultra-fine WC-Co-Cr3C2 cemented carbides via an approach based on thermodynamic calculations and characterization of the experimental results by the Weibull distribution. Calphad: Computer Coupling of Phase Diagrams and Thermochemistry, 2020, 70, 101778.	0.7	10
431	Diffusivities and Atomic Mobilities for the Cu-Rich fcc Cu-Al-Sn Alloys at 1073ÂK. Journal of Phase Equilibria and Diffusion, 2020, 41, 378-389.	0.5	10
432	Assessment of atomic mobilities and simulation of precipitation evolution in Mg-X (X=Al, Zn, Sn) alloys. Journal of Materials Science and Technology, 2021, 62, 70-82.	5.6	10

#	Article	IF	CITATIONS
433	Experimental investigation and CALPHAD modeling of the Cu–Cr–Si ternary system. Calphad: Computer Coupling of Phase Diagrams and Thermochemistry, 2021, 74, 102324.	0.7	10
434	Thermodynamic assessment of the YO1.5î—,MgO system. Journal of Alloys and Compounds, 1991, 176, L1-L4.	2.8	9
435	A thermodynamic description of the Al–Be system: Modeling and experiment. Calphad: Computer Coupling of Phase Diagrams and Thermochemistry, 2004, 28, 371-378.	0.7	9
436	Crystallization of Al ₂ FeZr ₆ Amorphous Alloy Prepared by Mechanical Alloying. Materials Transactions, 2006, 47, 388-391.	0.4	9
437	Reassessment of the Ni–B system supported by key experiments and first-principles calculation. International Journal of Materials Research, 2009, 100, 59-67.	0.1	9
438	First-principles studies on structural and electronic properties of TaCr2 Laves phase. Physica B: Condensed Matter, 2010, 405, 4279-4282.	1.3	9
439	Isothermal section of the Cu–Mn–Si ternary system at 700 °C. Journal of Alloys and Compounds, 2010, 492, 190-195.	2.8	9
440	Experimental investigation and thermodynamic modeling of the Mg–Si–Zn system. Calphad: Computer Coupling of Phase Diagrams and Thermochemistry, 2011, 35, 183-190.	0.7	9
441	Properties of hexagonal Al2Ge2REÂ(RE=Y,La,Ce,Nd,Eu,Gd,Tb,Y bÂandÂLu) : A first-principles study. Solid State Communications, 2011, 151, 1814-1819.	0.9	9
442	The structural, electronic, elastic and optical properties of AlCu(Se1â^'Te)2 compounds from first-principle calculations. Current Applied Physics, 2012, 12, 373-379.	1.1	9
443	A New Diffusivity Database for Multi-Component Al Alloys: Focusing on Ternary Systems and its Effect on Microstructure Evolution during Solidification. Materials Science Forum, 0, 794-796, 611-616.	0.3	9
444	Temperature-dependent elastic stiffness constants of fcc-based metal nitrides from first-principles calculations. Journal of Materials Science, 2014, 49, 424-432.	1.7	9
445	Diffusivities and atomic mobilities in fcc Pt–Al alloys. Calphad: Computer Coupling of Phase Diagrams and Thermochemistry, 2014, 46, 118-123.	0.7	9
446	Thermal analysis and microstructural investigation of Cu-rich alloys in the Cu–Al–Ag system. Journal of Alloys and Compounds, 2014, 612, 486-492.	2.8	9
447	Diffusivities and atomic mobilities in disordered fcc and ordered L12 Ni–Al–W alloys. Journal of Alloys and Compounds, 2015, 645, 259-268.	2.8	9
448	Measurement of 900°C Isothermal Section in the Mo-Ni-Zr System. Journal of Phase Equilibria and Diffusion, 2016, 37, 672-679.	0.5	9
449	Asymmetric mixing behavior and stability of the predicted phases in the W–Cu system. Calphad: Computer Coupling of Phase Diagrams and Thermochemistry, 2016, 53, 116-121.	0.7	9
450	Experimental investigation on the phase equilibria of the Mg-Sn-Ag system in the Mg-rich corner. Journal of Magnesium and Alloys, 2017, 5, 41-47.	5.5	9

Үомс Du

#	Article	IF	CITATIONS
451	Thermodynamic assessment of the C–Zr–Nb ternary system. Calphad: Computer Coupling of Phase Diagrams and Thermochemistry, 2018, 61, 98-104.	0.7	9
452	A thermodynamic description of the Uâ^'Tiâ^'Zr system. Calphad: Computer Coupling of Phase Diagrams and Thermochemistry, 2018, 60, 90-97.	0.7	9
453	Numerical simulation of kinetic demixing and decomposition in a LaCoO3-l̂ ² oxygen membrane under an oxygen potential gradient. Journal of Membrane Science, 2018, 548, 526-539.	4.1	9
454	Assessment of atomic mobilities for fcc Co–Ti–V alloys. Calphad: Computer Coupling of Phase Diagrams and Thermochemistry, 2018, 61, 179-188.	0.7	9
455	Kinetic Phase Diagrams of Ternary Al-Cu-Li System during Rapid Solidification: A Phase-Field Study. Materials, 2018, 11, 260.	1.3	9
456	Measurement of the Interdiffusion Coefficients in Mo-Ti and Mo-Ti-Zr Beta Phase Alloys from 1273 to 1473ÂK. Journal of Phase Equilibria and Diffusion, 2019, 40, 206-218.	0.5	9
457	Precipitation of γ′ in the γ binder phase of WC-Al-Co-Ni cemented carbide: A phase-field study. Calphad: Computer Coupling of Phase Diagrams and Thermochemistry, 2020, 68, 101717.	0.7	9
458	Atomic mobilities and diffusivities in fcc_A1 Ni–Cr–V system: Modeling and application. Calphad: Computer Coupling of Phase Diagrams and Thermochemistry, 2020, 70, 101808.	0.7	9
459	Measurements of the melting points, liquidus, and solidus of the Mo, Ta, and Mo Ta binary alloys using a novel high-speed pyrometric technique. International Journal of Refractory Metals and Hard Materials, 2020, 93, 105335.	1.7	9
460	Diffusion coefficients and atomic mobilities in fcc Ni–Cu–Mo alloys: Experiment and modeling. Calphad: Computer Coupling of Phase Diagrams and Thermochemistry, 2020, 71, 102209.	0.7	9
461	Thermal Conductivity of As-Cast and Annealed Mg-RE Binary Alloys. Metals, 2021, 11, 554.	1.0	9
462	Computational engineering of the oxygen electrode-electrolyte interface in solid oxide fuel cells. Npj Computational Materials, 2021, 7, .	3.5	9
463	Interdiffusion and atomic mobility in hcp Mg–Al–Sn alloys. Journal of Alloys and Compounds, 2021, 871, 159517.	2.8	9
464	Interdiffusion behaviors and mechanical properties of Zn–Cr system. Calphad: Computer Coupling of Phase Diagrams and Thermochemistry, 2021, 74, 102308.	0.7	9
465	Fabrication of gradient cemented carbide with Ni3Al binder: Simulations and experiments. Ceramics International, 2022, 48, 12756-12763.	2.3	9
466	Experimental and thermodynamic investigations in the Tiâ€6iâ€C system. Zeitschrift Fur Elektrotechnik Und Elektrochemie, 1998, 102, 1185-1188.	0.9	8
467	Thermodynamic investigation of the KBr–TbBr3 system. Calphad: Computer Coupling of Phase Diagrams and Thermochemistry, 2008, 32, 43-48.	0.7	8
468	Density functional study of 3d-transition metal aluminides. Computational and Theoretical Chemistry, 2009, 905, 106-112.	1.5	8

Үомс Du

#	Article	IF	CITATIONS
469	Phase equilibria of the Co–Ta–Ti system at 950°C. Journal of Alloys and Compounds, 2009, 485, 249-254.	2.8	8
470	Effect of fabrication parameters on the microstructure, in-plane anisotropy and magnetostriction of Fe-Ga thin films. Rare Metals, 2010, 29, 583-588.	3.6	8
471	Reassessment of the Mg–Ge binary system using CALPHAD supported by first-principles calculation. International Journal of Materials Research, 2010, 101, 1489-1496.	0.1	8
472	Determination of the phase equilibria in the Al–Er–V ternary system at 773K. Journal of Alloys and Compounds, 2010, 503, 61-64.	2.8	8
473	Interdiffusivities and atomic mobilities in fcc Cu–Al–Fe alloys. Calphad: Computer Coupling of Phase Diagrams and Thermochemistry, 2011, 35, 556-561.	0.7	8
474	Phase equilibria of the Ni–Si–Zn system at 600°C. Intermetallics, 2011, 19, 1089-1095.	1.8	8
475	Numerical computations for temperature, fraction of solid phase and composition couplings in ternary alloy solidification with three different thermodynamic data-acquisition methods. Calphad: Computer Coupling of Phase Diagrams and Thermochemistry, 2012, 36, 155-162.	0.7	8
476	Thermodynamic assessment of the Ga–X (X=B, Ca, Sr, Ba) systems supported by first-principles calculations. Calphad: Computer Coupling of Phase Diagrams and Thermochemistry, 2013, 43, 52-60.	0.7	8
477	Effect of liquid diffusion coefficients on microstructure evolution during solidification of Al356.1 alloy. Transactions of Nonferrous Metals Society of China, 2013, 23, 3722-3728.	1.7	8
478	Constitution of the ternary system Cr–Ni–Ti. Journal of Alloys and Compounds, 2013, 575, 48-53.	2.8	8
479	First-principles investigation of the mechanical, electronic and thermophysical properties of Q-phase in Al–Mg–Si–Cu alloys. Computational Materials Science, 2013, 67, 334-340.	1.4	8
480	Experimental Investigation on Phase Equilibria of Al-Fe-Y System at 773ÂK. Journal of Phase Equilibria and Diffusion, 2014, 35, 256-261.	0.5	8
481	Application of CALPHAD approach in simulation of liquid phase migration of cellular cemented carbide. International Journal of Refractory Metals and Hard Materials, 2014, 42, 180-184.	1.7	8
482	Thermodynamic modeling of the Ca–In and Ca–Sb systems supported with first-principles calculations. Calphad: Computer Coupling of Phase Diagrams and Thermochemistry, 2015, 48, 35-42.	0.7	8
483	Interdiffusion in bcc_B2 Ni–Al–Cu alloys at 1 173 K. International Journal of Materials Research, 2016, 107, 597-604.	0.1	8
484	Diffusivities and atomic mobilities in Sn–Ag–In and Sn–Ag–Sb melts. Calphad: Computer Coupling of Phase Diagrams and Thermochemistry, 2016, 52, 159-168.	0.7	8
485	Effect of stamping deformation on microstructure and properties evolution of an Al–Mg–Si–Cu alloy for automotive panels. Journal of Materials Science, 2017, 52, 5569-5581.	1.7	8
486	Experimental investigation and thermodynamic assessment of the Li-Sb system. Calphad: Computer Coupling of Phase Diagrams and Thermochemistry, 2017, 57, 28-36.	0.7	8

#	Article	IF	CITATIONS
487	Phase diagram of the quaternary system LiCl+MgCl2+KCl+H2O at 323.15 K. Calphad: Computer Coupling of Phase Diagrams and Thermochemistry, 2017, 57, 126-133.	0.7	8
488	Effect of WC and Co on the Microstructure and Properties of TiC Steel-Bonded Carbide. Materials Science Forum, 0, 898, 1468-1477.	0.3	8
489	Reassessment of the Ni–V system and a new thermodynamic modeling of the Mo–Ni–V system. Thermochimica Acta, 2018, 661, 137-146.	1.2	8
490	Thermodynamic Assessment of the Ti-RE (REÂ=ÂCe, Er, Tm, Y) Binary Systems. Journal of Phase Equilibria and Diffusion, 2018, 39, 44-50.	0.5	8
491	Effect of Different Initial Structures on the Simulation of Microstructure Evolution During Normal Grain Growth via Phase-Field Modeling. Metallurgical and Materials Transactions A: Physical Metallurgy and Materials Science, 2018, 49, 6442-6456.	1.1	8
492	Experimental Investigation of the Mo–Ti–Zr Ternary Phase Diagrams. Journal of Phase Equilibria and Diffusion, 2018, 39, 789-799.	0.5	8
493	Experimental Chemistry and Structural Stability of AlNb3 Enabled by Antisite Defects Formation. Materials, 2019, 12, 1104.	1.3	8
494	Thermodynamic description and simulation of solidification microstructure in the Co-Ti system. Journal of Chemical Thermodynamics, 2020, 142, 105995.	1.0	8
495	Thermodynamic description and phase selection for the Mo–Ti–Zr biomedical alloys. Calphad: Computer Coupling of Phase Diagrams and Thermochemistry, 2020, 70, 101799.	0.7	8
496	The interdiffusivity matrices in fcc_A1 Ni–Cr–V alloys: A high-throughput evaluation by CALTPP program. Calphad: Computer Coupling of Phase Diagrams and Thermochemistry, 2021, 72, 102229.	0.7	8
497	Thermodynamic description and simulation of solidification microstructures in the Cu–Mg–Zn system. Journal of Materials Science, 2021, 56, 10614-10639.	1.7	8
498	Development of multilayer graded cemented carbides with Ti–Zr carbonitride miscibility gaps. Ceramics International, 2021, 47, 7521-7527.	2.3	8
499	3D phase field modeling of the morphology of WC grains in WC–Co alloys: The role of interface anisotropy. Computational Materials Science, 2021, 196, 110526.	1.4	8
500	Experimental investigation and thermodynamic modeling of the Cu–Ag–Si ternary system. Journal of Chemical Thermodynamics, 2020, 150, 106172.	1.0	8
501	Impact of oxygen content on the thermal stability of Ti-Al-O-N coatings based on computational and experimental studies. Acta Materialia, 2022, 227, 117706.	3.8	8
502	Experimental investigation, thermodynamic modeling and solidified microstructure of the Cu–Ti–Nb ternary system. Calphad: Computer Coupling of Phase Diagrams and Thermochemistry, 2022, 76, 102395.	0.7	8
503	Comment on "Thermodynamic Properties of Cerium Oxalate and Cerium Oxide". Journal of the American Ceramic Society, 1994, 77, 2783-2784.	1.9	7
504	Thermodynamic reassessment of the Cu–V system supported by key experiments. Calphad: Computer Coupling of Phase Diagrams and Thermochemistry, 2008, 32, 252-255.	0.7	7

#	Article	IF	CITATIONS
505	The elastic constants for Fe ₃ AlX (X=B, C and N) with anti-perovskite structure. Physica Scripta, 2009, 80, 055603.	1.2	7
506	Thermodynamic Assessment of the Cu-B System Supported by Key Experiment and First-Principles Calculations. Journal of Phase Equilibria and Diffusion, 2009, 30, 480-486.	0.5	7
507	A thermodynamic description of the Ge–Sr system acquired via a hybrid approach of CALPHAD and first-principles calculations. Calphad: Computer Coupling of Phase Diagrams and Thermochemistry, 2009, 33, 719-722.	0.7	7
508	The isothermal section of the Pr–Ti–Si ternary system at 773K. Journal of Alloys and Compounds, 2009, 479, 201-203.	2.8	7
509	Phase equilibria of the Ag–Gd–Sn ternary system at 400°C. Journal of Alloys and Compounds, 2009, 481, 264-269.	2.8	7
510	Thermodynamic Assessment of the Mn-B System. Journal of Phase Equilibria and Diffusion, 2010, 31, 357-364.	0.5	7
511	Energetic, mechanical, and vibrational stability of metastable OsC phase. Journal of Applied Physics, 2010, 108, .	1.1	7
512	Phase equilibria of the Al–Pr–Zr ternary system at 773K. Journal of Alloys and Compounds, 2010, 503, 57-60.	2.8	7
513	Diffusivities and atomic mobilities in Cu-rich fcc Al–Cu–Mn alloys. International Journal of Materials Research, 2012, 103, 807-813.	0.1	7
514	Phase-field Simulation of Microstructural Evolution of γ Precipitate in γ′ Matrix in Binary Ni-Al Alloys. Procedia Engineering, 2012, 36, 200-206.	1.2	7
515	Experimental Investigation of the Al-Cr-Gd Ternary System at 773ÂK. Journal of Phase Equilibria and Diffusion, 2012, 33, 203-209.	0.5	7
516	Phase Equilibria of the Al–V–RE (REÂ=ÂGd, Ho) Systems at 773ÂK (500°C). Metallurgical and Materials Transactions A: Physical Metallurgy and Materials Science, 2012, 43, 29-36.	1.1	7
517	Interdiffusivities and Atomic Mobilities in fcc Ni-Cu-Si Alloys. Journal of Phase Equilibria and Diffusion, 2013, 34, 484-492.	0.5	7
518	Thermodynamic assessment of the Sr–In and Sr–Bi systems supported by first-principles calculations. Calphad: Computer Coupling of Phase Diagrams and Thermochemistry, 2014, 45, 49-54.	0.7	7
519	First-principles calculations of finite-temperature thermodynamic properties of binary solid solutions in the Al–Cu–Mg system. Calphad: Computer Coupling of Phase Diagrams and Thermochemistry, 2014, 47, 196-210.	0.7	7
520	Thermodynamic Assessment of the Bi–Ni and Bi–Ni–X (XÂ=ÂAg, Cu) Systems. Journal of Electronic Materials, 2016, 45, 1041-1056.	1.0	7
521	First-Principles Study of Intrinsic Defects in Ammonia Borane. Journal of Physical Chemistry C, 2017, 121, 22680-22689.	1.5	7
522	Experimental investigation and thermodynamic assessment of the Mo–Ni–Zr ternary system. Calphad: Computer Coupling of Phase Diagrams and Thermochemistry, 2017, 58, 128-137.	0.7	7

#	Article	IF	CITATIONS
523	Phase-field simulation of the solidified microstructure in a new commercial 6××× aluminum alloy ingot supported by experimental measurements. International Journal of Materials Research, 2018, 109, 91-98.	0.1	7
524	A stepwise thermodynamic modeling of the phase diagram for the Cu–Be system. Journal of Materials Science, 2018, 53, 3756-3766.	1.7	7
525	Cu–Fe–Co System: Verification of the High-Temperature Phase Equilibria and Thermodynamic Modeling of the Low-Temperature Phase Relations Involving Ordered Phase. Powder Metallurgy and Metal Ceramics, 2018, 56, 546-555.	0.4	7
526	Atomic mobility evaluation and diffusion matrix for fcc_A1 Co–V–W alloys. Journal of Materials Science, 2019, 54, 13420-13432.	1.7	7
527	Thermodynamic modeling of the U-Nb-Zr ternary system. Journal of Nuclear Materials, 2019, 523, 157-171.	1.3	7
528	Experimental Investigation of the Mg–Zn–Zr Isothermal Section at 400°C. Acta Metallurgica Sinica (English Letters), 2019, 32, 426-432.	1.5	7
529	Effect of electron beam irradiation in TEM on the microstructure and composition of nanoprecipitates in Al-Mg-Si alloys. Micron, 2019, 116, 116-123.	1.1	7
530	Diffusivity and Atomic Mobility in fcc Ni-Fe-V System: Experiment and Modeling. Journal of Phase Equilibria and Diffusion, 2020, 41, 550-566.	0.5	7
531	Effect of alloying on stability of grain boundary in γ phase of the U–Mo and U–Nb systems. Calphad: Computer Coupling of Phase Diagrams and Thermochemistry, 2021, 72, 102241.	0.7	7
532	Thermodynamic re-assessment and liquidus projection of the Cu–Ni–Ti system. Calphad: Computer Coupling of Phase Diagrams and Thermochemistry, 2021, 73, 102256.	0.7	7
533	Microstructure, hardness and interfacial energy in Co-9Al-10W-xNi (x=15, 25, 35 at. %) alloys during aging. Journal of Mining and Metallurgy, Section B: Metallurgy, 2017, 53, 303-308.	0.3	7
534	Interdiffusion behaviors and mechanical properties in BCC Zr-rich Zr–Nb–Ta system. Calphad: Computer Coupling of Phase Diagrams and Thermochemistry, 2022, 77, 102410.	0.7	7
535	A reassessment of the ZrO2î—,YO1·5î—,MgO system. Ceramics International, 1994, 20, 17-25.	2.3	6
536	Theoretical study of spectroscopic parameters of alkali -Al and alkaline earth-Al dimers. Theoretical Chemistry Accounts, 2008, 121, 165-172.	0.5	6
537	Thermodynamic Modeling of the Sr-M (MÂ=ÂFe, Mn, Ni, Ti, V) Systems. Journal of Phase Equilibria and Diffusion, 2011, 32, 42-47.	0.5	6
538	Experimental Phase Diagram of the Al-Er-Zr Ternary System. Journal of Phase Equilibria and Diffusion, 2011, 32, 412-417.	0.5	6
539	Thermodynamic modeling of the Sr–X (X=H, Li, Na, Sc) systems. Calphad: Computer Coupling of Phase Diagrams and Thermochemistry, 2012, 38, 17-22.	0.7	6
540	Thermodynamic assessment of the Sn–Sr system supported by first-principles calculations. Thermochimica Acta, 2012, 529, 74-79.	1.2	6

#	Article	IF	CITATIONS
541	Diffusivities and atomic mobilities in the Al–Ce–Ni melts. Journal of Non-Crystalline Solids, 2013, 379, 201-207.	1.5	6
542	Experimental Investigation and Thermodynamic Modeling of the Nd-Zr and the Mg-Nd-Zr Systems. Metallurgical and Materials Transactions A: Physical Metallurgy and Materials Science, 2014, 45, 2708-2718.	1.1	6
543	Experimental investigation and thermodynamic modeling of the Ga–Zr system. Journal of Alloys and Compounds, 2014, 587, 497-505.	2.8	6
544	Prediction of diffusivities in fcc phase of the Al–Cu–Mg system: First-principles calculations coupled with CALPHAD technique. Computational Materials Science, 2014, 90, 32-43.	1.4	6
545	Heat contents of Sc5Si3 and ScSi intermetallics and thermodynamic modeling of the Sc–Si system. Journal of Thermal Analysis and Calorimetry, 2015, 119, 1315-1321.	2.0	6
546	Thermodynamic Description of the Al-Fe-Mg-Ni-Si and Al-Cu-Fe-Mg-Ni Quinary Systems and Its Application to Solidification Simulation. Journal of Phase Equilibria and Diffusion, 2015, 36, 333-349.	0.5	6
547	A thermodynamic description of the C–Ti–V system over the whole composition and temperature ranges. International Journal of Refractory Metals and Hard Materials, 2015, 48, 346-354.	1.7	6
548	Experimental investigation of the isothermal section at 400 °C of the MgCeSr ternary system. Journal of Magnesium and Alloys, 2016, 4, 30-35.	5.5	6
549	Mechanical properties of β″ precipitates containing Al and/or Cu in age hardening Al alloys. Journal of Materials Research, 2016, 31, 580-588.	1.2	6
550	A New Relationship Among Self- and Impurity Diffusion Coefficients in Binary Solution Phases. Metallurgical and Materials Transactions A: Physical Metallurgy and Materials Science, 2016, 47, 3295-3299.	1.1	6
551	Phase-field simulation of liquid phase migration in the WC–Co system during liquid phase sintering. International Journal of Materials Research, 2016, 107, 309-314.	0.1	6
552	Experimental Investigation and Thermodynamic Calculations of the Co-Fe-Ti System. Journal of Phase Equilibria and Diffusion, 2017, 38, 5-16.	0.5	6
553	A Thermodynamic Assessment of the Li-Ge System. Journal of Phase Equilibria and Diffusion, 2018, 39, 315-323.	0.5	6
554	Microstructure and mechanical properties of ultra-fine WC-10Co cemented carbides with Cr3C2 and NbC: Experimental investigation supported by thermodynamic calculation. International Journal of Materials Research, 2018, 109, 284-290.	0.1	6
555	Thermodynamic descriptions of the Ag-X (X = S, As, Lu) systems. Calphad: Computer Coupling of Phase Diagrams and Thermochemistry, 2018, 62, 207-214.	0.7	6
556	Modelling the viscosity of liquid alloys with associates. Journal of Molecular Liquids, 2019, 291, 111345.	2.3	6
557	CALPHAD-type modeling of the C–Hf–Mo system over the whole composition and temperature ranges. Thermochimica Acta, 2020, 692, 178716.	1.2	6
558	Phase equilibria and crystal structure of ternary compounds in Al-rich corner of Al-Er-Y system at 673 and 873K. Journal of Materials Science and Technology, 2021, 60, 128-138.	5.6	6

#	Article	IF	CITATIONS
559	Experimental Investigation and Thermodynamic Modeling of the Phase Equilibria in the Cu-Nb-Ni Ternary System. Journal of Phase Equilibria and Diffusion, 2021, 42, 150-163.	0.5	6
560	Understanding the surface adsorption and oxidation of cubic Cr0.5Al0.5N by first-principles calculations. Computational Materials Science, 2021, 196, 110518.	1.4	6
561	Thermodynamic modeling of the Te-X (X = Zr, Ce, Eu) systems. Calphad: Computer Coupling of Phase Diagrams and Thermochemistry, 2021, 74, 102281.	0.7	6
562	High-throughput exploration of the composition-dependent elasto-plastic properties in Co–Ni–W system. Journal of Alloys and Compounds, 2022, 896, 163061.	2.8	6
563	Investigation of mechanical and diffusion properties in bcc Tiâ^'Nbâ^'Zrâ^'Sn alloys via a high-throughput method. Transactions of Nonferrous Metals Society of China, 2021, 31, 3405-3415.	1.7	6
564	Phase equilibria of the Co–Mo–Ti system at 950°C. Journal of Alloys and Compounds, 2008, 457, 259-264.	2.8	5
565	Electronic calculation of Mn3AlN with anti-perovskite structure. Computational Materials Science, 2008, 44, 97-101.	1.4	5
566	The phase equilibria in the Nd–Ti–Si ternary system at 773K. Journal of Alloys and Compounds, 2009, 477, 274-277.	2.8	5
567	The phase equilibria in the Gd–Ti–Fe ternary system at 773K. Journal of Alloys and Compounds, 2009, 485, 196-199.	2.8	5
568	Simulation of the ultra-fine microstructure evolution during annealing of AZ31 processed by ECAP. Physica B: Condensed Matter, 2010, 405, 1969-1972.	1.3	5
569	Study of diffusion and atomic mobilities for fcc Ag–Cd and Ag–Sn solder alloys. Calphad: Computer Coupling of Phase Diagrams and Thermochemistry, 2011, 35, 224-230.	0.7	5
570	Phase Diagrams of the Ce-Si-Zr Ternary System at 773 and 1173ÂK. Journal of Phase Equilibria and Diffusion, 2011, 32, 435-440.	0.5	5
571	Heat contents of the intermetallics V3Ce and V5Ce3 and thermodynamic modeling of the Ge–V system. Thermochimica Acta, 2011, 513, 100-105.	1.2	5
572	Phase boundary migration, Kirkendall marker shift and atomic mobilities in fcc Au–Pt alloys. Calphad: Computer Coupling of Phase Diagrams and Thermochemistry, 2012, 36, 94-99.	0.7	5
573	Experimental Investigation and Thermodynamic Assessment of the Hf-Mn System. Journal of Phase Equilibria and Diffusion, 2012, 33, 20-28.	0.5	5
574	Experimental investigation and thermodynamic description of the Mg–Y–Zr system. Journal of Materials Science, 2014, 49, 7124-7132.	1.7	5
575	Atomic mobilities in fcc Cu–Mn–Ni–Zn alloys and their characterizations of uphill diffusion and zero-flux plane phenomena. International Journal of Materials Research, 2014, 105, 13-31.	0.1	5
576	Experimental investigation and thermodynamic calculation of the Mg–Mn–Ni system. Calphad: Computer Coupling of Phase Diagrams and Thermochemistry, 2015, 49, 41-49.	0.7	5

#	Article	IF	CITATIONS
577	Revisiting the thermodynamic properties of the LiCl–NaCl–KCl–H2O quaternary and its sub-ternary systems at 298.15 K. Calphad: Computer Coupling of Phase Diagrams and Thermochemistry, 2015, 50, 161-169.	0.7	5
578	Modeling of Ni Diffusion Induced Austenite Formation in Ferritic Stainless Steel Interconnects. ECS Transactions, 2015, 68, 1691-1700.	0.3	5
579	Microstructure evolution in multilayer c-TiAlN/TiN coatings during spinodal decomposition — A phase-field study. Journal of Micromechanics and Molecular Physics, 2016, 01, 1650002.	0.7	5
580	Experimental investigation and thermodynamic modeling of the Ce-Si system. Thermochimica Acta, 2016, 646, 49-58.	1.2	5
581	Thermodynamic calculations of the Au–Sc and Fe–Sc systems. Calphad: Computer Coupling of Phase Diagrams and Thermochemistry, 2016, 54, 158-164.	0.7	5
582	Phase equilibria in the ternary B-Ce-Cu system with a thermodynamic reassessment of the binary B-Ce system. Thermochimica Acta, 2017, 657, 185-196.	1.2	5
583	Thermodynamic Reassessment of the C-Ni-Si System Using a Four Sublattice Model for Ordered/Disordered fcc Phases. Journal of Phase Equilibria and Diffusion, 2017, 38, 807-813.	0.5	5
584	The Evolution of Second-Phase Particles in 6111 Aluminum Alloy Processed by Hot and Cold Rolling. Journal of Materials Engineering and Performance, 2018, 27, 1130-1137.	1.2	5
585	Interdiffusion Coefficients in FCC Co-Rich Co-Ti-V Alloys at 1273, 1373 and 1473ÂK. Journal of Phase Equilibria and Diffusion, 2018, 39, 109-116.	0.5	5
586	Understanding of hydrogen desorption mechanism from defect point of view. National Science Review, 2018, 5, 318-320.	4.6	5
587	Interdiffusion and Atomic Mobilities of fcc Co-V-Mo Alloys: Measurement and Modeling. Journal of Phase Equilibria and Diffusion, 2018, 39, 623-634.	0.5	5
588	Thermodynamic Description of the Al–X (X = S, Se, Te) Systems. Journal of Phase Equilibria and Diffusion, 2019, 40, 392-402.	0.5	5
589	Numerical Simulation of the SrZrO3 Formation in Solid Oxide Fuel Cells. Journal of Electronic Materials, 2019, 48, 5510-5515.	1.0	5
590	A new algorithm to calculate binary phase diagrams. Computational Materials Science, 2019, 159, 478-483.	1.4	5
591	Thermodynamic Modeling of the Ag-X (X = B, Fe, Sm, Pu) Binary Systems. Journal of Phase Equilibria and Diffusion, 2020, 41, 257-268.	0.5	5
592	On the temperature-dependent diffusion growth of ï⊷Mg5Al2Zn2 ternary intermetallic compound in the Mg–Al–Zn system. Journal of Materials Science, 2021, 56, 3488-3497.	1.7	5
593	Thermodynamics Controlled Sharp Transformation from InP to GaP Nanowires via Introducing Trace Amount of Gallium. Nanoscale Research Letters, 2021, 16, 49.	3.1	5
594	Phase equilibria thermodynamics and solidified microstructure in the Ag-Cr-Zr system. Journal of Alloys and Compounds, 2021, 863, 158618.	2.8	5

#	Article	IF	CITATIONS
595	Influence of Si doping on the microstructure and hardness of an AlTiSiN coating deposited by low pressure chemical vapor deposition. Ceramics International, 2021, 47, 25593-25601.	2.3	5
596	A thermodynamic description of metastable c-TiAlZrN coatings with triple spinodally decomposed domains. Journal of Mining and Metallurgy, Section B: Metallurgy, 2017, 53, 85-93.	0.3	5
597	Diffusivity and atomic mobility in fcc Cu–Mn–Si alloys: measurements and modeling by CALTPP program. Journal of Materials Science, 2022, 57, 5241-5257.	1.7	5
598	Interdiffusion behaviors and mechanical properties of Zr-X (X Nb, Ta, Hf) binary systems. Journal of Alloys and Compounds, 2022, 910, 164910.	2.8	5
599	Thermodynamic Modelling of the Te-X (X = Cu, Ga, Li, Sr) Systems. Journal of Phase Equilibria and Diffusion, 2022, 43, 193-213.	0.5	5
600	Calculation and application of liquidus projection. Rare Metals, 2006, 25, 532-537.	3.6	4
601	Phase diagram of the Co–Cu–Ti system at 850°C. International Journal of Materials Research, 2006, 97, 140-144.	0.1	4
602	The compositional range of amorphous phase formation and thermal stability of Al90â^'xFe5Ni5Cex. Journal of Alloys and Compounds, 2008, 460, 309-313.	2.8	4
603	Synthesis and electrochemical properties of Li[Ni x Co y Mn1â^'xâ^'y]O2(x, y = 2/8, 3/8) cathode materials for lithium ion batteries. Rare Metals, 2009, 28, 43-48.	3.6	4
604	First-principles study for surface tension and depolarizing effect on ferroelectric properties of BaTiO3 nanowires. Transactions of Nonferrous Metals Society of China, 2009, 19, 1634-1638.	1.7	4
605	The formation and crystallization for amorphous AlFeZr4 prepared by mechanical alloying. Physica B: Condensed Matter, 2010, 405, 2005-2008.	1.3	4
606	Interactions of the components in the Al–V–Nd system at 773K. Journal of Alloys and Compounds, 2010, 506, 589-592.	2.8	4
607	Assessment of Atomic Mobilities in fcc Al-Ag-Zn Alloys. Journal of Phase Equilibria and Diffusion, 2011, 32, 512-524.	0.5	4
608	First-principles calculations on the crystal, electronic structures and elastic properties of Ag-rich γ′ phase approximates in Al–Ag alloys. Computational Materials Science, 2012, 51, 415-421.	1.4	4
609	Comparison of Microstructure and Mechanical Properties of Co-Based and Fe-Based Alloy Coatings Deposited by PTA. Advanced Materials Research, 0, 834-836, 617-622.	0.3	4
610	Experimental Investigation of the Al-Fe-Nd System at 773ÂK. Journal of Phase Equilibria and Diffusion, 2014, 35, 86-92.	0.5	4
611	Thermodynamic assessment of the Cd–X (X=Sn, Mn, Fe) systems. Calphad: Computer Coupling of Phase Diagrams and Thermochemistry, 2014, 47, 83-91.	0.7	4
612	Ti and Ni Grain Boundary Diffusion in B2 NiTi Compound. Defect and Diffusion Forum, 2015, 363, 137-141.	0.4	4

#	Article	IF	CITATIONS
613	Mechanical properties and spinodal decomposition of Ti Al1â^'â^'Zr N coatings. Physics Letters, Section A: General, Atomic and Solid State Physics, 2015, 379, 2037-2040.	0.9	4
614	The microstructure evolution of U1 and U2 nanowires constrained in Al matrix. Computational Materials Science, 2016, 117, 180-187.	1.4	4
615	Experimental investigation and thermodynamic calculation of the Mg–Mn–Sr system. Calphad: Computer Coupling of Phase Diagrams and Thermochemistry, 2016, 52, 110-119.	0.7	4
616	Phase Equilibria of the Al-Sc-Zr Ternary System at 500°C. Journal of Phase Equilibria and Diffusion, 2017, 38, 493-501.	0.5	4
617	Experimental investigation and thermodynamic calculation of the Cu-Ge-Sb system. Journal of Alloys and Compounds, 2017, 726, 820-832.	2.8	4
618	Thermodynamic Assessment of the Mn-H and Mg-Mn-H Systems. Journal of Phase Equilibria and Diffusion, 2018, 39, 186-195.	0.5	4
619	Investigation of WC–Co alloy properties based on thermodynamic calculation and Weibull distribution. Materials Science and Technology, 2019, 35, 2269-2274.	0.8	4
620	Thermodynamic modeling of the chromium-yttrium-oxygen system. Calphad: Computer Coupling of Phase Diagrams and Thermochemistry, 2019, 64, 1-10.	0.7	4
621	Phase-field simulation of solidification microstructure in Ni and Cu–Ni alloy using the Wheeler, Boettinger and McFadden model coupled with the CALPHAD data. Calphad: Computer Coupling of Phase Diagrams and Thermochemistry, 2020, 68, 101691.	0.7	4
622	Critical evaluation of ternary phase diagram data: Important considerations in the scrutiny of the correctness, coherence, and interpretation. Calphad: Computer Coupling of Phase Diagrams and Thermochemistry, 2020, 68, 101719.	0.7	4
623	Solid-solubilities of grain-growth inhibitors in WC-Ni-based cemented carbides: experimental investigations and thermodynamic calculations. Journal of Materials Research and Technology, 2020, 9, 10346-10354.	2.6	4
624	Phase equilibria and thermodynamic investigation of the In–Li system. Calphad: Computer Coupling of Phase Diagrams and Thermochemistry, 2020, 70, 101779.	0.7	4
625	Phase equilibria of the Cu–Zr–Si system at 750 and 900°C. Calphad: Computer Coupling of Phase Diagrams and Thermochemistry, 2020, 68, 101727.	0.7	4
626	Thermodynamic re-assessment and experimental confirmation for the Zn–Mn system. Calphad: Computer Coupling of Phase Diagrams and Thermochemistry, 2020, 69, 101770.	0.7	4
627	Experimental investigation and thermodynamic modeling of the U–Nb system. Journal of Materials Science and Technology, 2021, 81, 229-235.	5.6	4
628	Experimental investigation of the Ni-V-W ternary phase diagrams. Calphad: Computer Coupling of Phase Diagrams and Thermochemistry, 2022, 76, 102384.	0.7	4
629	Discovery of a bulk C36-type MgZn2 structure step by step transformed from the C14 prototype laves phase structure. Journal of Materials Science, 2022, 57, 2999-3009.	1.7	4
630	Combined Thermal Runaway Investigation of Coin Cells with an Accelerating Rate Calorimeter and a Tian-Calvet Calorimeter. Batteries, 2022, 8, 15.	2.1	4

Үомс Du

#	Article	IF	CITATIONS
631	Thermodynamic modeling of the gadolinium–germanium system. Journal of Alloys and Compounds, 2008, 462, 181-186.	2.8	3
632	Structure and stability of Al–Fe–Zr–Ce cluster: density functional study. Theoretical Chemistry Accounts, 2010, 127, 651-659.	0.5	3
633	Experimental investigation and thermodynamic modeling of the Cu–Mn–Zn system. International Journal of Materials Research, 2010, 101, 1376-1391.	0.1	3
634	Elastic constants and thermophysical properties of Al–Mg–Si alloys from first-principles calculations. International Journal of Materials Research, 2010, 101, 1392-1397.	0.1	3
635	Isothermal section at 1100°C of the Fe–Ni–Ta system. Journal of Alloys and Compounds, 2010, 504, 181-185.	2.8	3
636	Phase equilibria and thermodynamic modeling in the Ge–Zr binary system. Journal of Materials Science, 2011, 46, 1405-1413.	1.7	3
637	Thermo-Calc and T—fS—CL coupling based method to determine solidification paths of alloys solidified under condition of Biotâ‰0.1. Transactions of Nonferrous Metals Society of China, 2012, 22, 139-146.	1.7	3
638	Structural, electronic, elastic and thermodynamic properties of CaAl2Zn2 compound under different pressures. Computational Materials Science, 2012, 59, 33-40.	1.4	3
639	Thermodynamic description of the Mn-Si-Zn system. Science China Technological Sciences, 2012, 55, 475-483.	2.0	3
640	Experimental Investigation of the Al-Fe-Gd System at 773ÂK. Journal of Phase Equilibria and Diffusion, 2013, 34, 116-121.	0.5	3
641	Phase diagram investigation of the Sn-In x Ag y Cu z (x:y:z = 7:2:1) section in the Ag-In-Sn-Cu system. International Journal of Materials Research, 2013, 104, 452-456.	0.1	3
642	The pressure dependences of elastic and lattice dynamic properties of AlAs fromab initiocalculations. Chinese Physics B, 2013, 22, 026201.	0.7	3
643	Structural, elastic and electronic properties of Cu-X compounds from first-principles calculations. Journal of Central South University, 2015, 22, 1585-1594.	1.2	3
644	Thermodynamic description and quaternary miscibility gap of the C–Hf–Ti–W system. Journal of Alloys and Compounds, 2017, 705, 581-589.	2.8	3
645	Experimental investigation and thermodynamic calculations of the Ag–Ga–Sn phase diagram. Calphad: Computer Coupling of Phase Diagrams and Thermochemistry, 2017, 56, 215-223.	0.7	3
646	Composition-dependent tracer diffusion coefficients in the B2 Ni–Al–Ti alloy via a combination of radiotracer and diffusion couple techniques. Journal of Alloys and Compounds, 2017, 720, 332-339.	2.8	3
647	Thermodynamic modeling of the Ta–Mo–C ternary system. Calphad: Computer Coupling of Phase Diagrams and Thermochemistry, 2017, 59, 99-106.	0.7	3
648	Phase relationship of the Ag–Zr–Cr system at 1000 and 750°C. International Journal of Materials Research, 2018, 109, 756-770.	0.1	3

Үомс Du

#	Article	IF	CITATIONS
649	Isothermal sections of the Co–Ni–Ti system at 950 and 1 000 °C. International Journal of Materials Research, 2018, 109, 105-112.	0.1	3
650	Thermodynamic Calculation of Phase Equilibria in the C-Mo-Zr System. Journal of Phase Equilibria and Diffusion, 2018, 39, 766-777.	0.5	3
651	Effects of hot rolling, intermediate annealing and cold rolling on microstructure, texture and mechanical properties of an Al-Mg-Si-Cu alloy. Materials Research Express, 2018, 5, 106521.	0.8	3
652	Phase Equilibria of the Ternary Al-Cu-Zn Alloys on Al-Zn Rich Side. Journal of Phase Equilibria and Diffusion, 2018, 39, 356-365.	0.5	3
653	Thermodynamic investigation of phase equilibria on the (W,Mo)C-(Co,Ni) cemented carbides. Calphad: Computer Coupling of Phase Diagrams and Thermochemistry, 2019, 67, 101664.	0.7	3
654	Thermodynamic modeling of the Ni–Nb–V ternary system. Calphad: Computer Coupling of Phase Diagrams and Thermochemistry, 2019, 67, 101673.	0.7	3
655	Thermodynamic Re-assessment of the Lanthanum-Tin System. Journal of Phase Equilibria and Diffusion, 2019, 40, 653-667.	0.5	3
656	Measurement of interdiffusivity for fcc_A1 Co-V-W alloys. International Journal of Refractory Metals and Hard Materials, 2020, 87, 105134.	1.7	3
657	A thermodynamic description of the C–Nb–Ti system over the whole composition and temperature ranges and its application in solidification microstructure analysis. Calphad: Computer Coupling of Phase Diagrams and Thermochemistry, 2020, 70, 101769.	0.7	3
658	Effect of annealing on the microstructure and mechanical properties of Ti0.17Al0.83N coating prepared by low pressure chemical vapor deposition. Surface and Coatings Technology, 2021, 412, 127014.	2.2	3
659	Stability, Elastic and Electronic Properties of Ta2N by First-Principles Calculations. Crystals, 2021, 11, 445.	1.0	3
660	Phase equilibria, crystal structure of δ1-MnZn9 and thermodynamic re-assessment of the Zn-Mn system. Journal of Alloys and Compounds, 2021, 863, 158484.	2.8	3
661	Thermodynamic assessment of the Ni-Co-M1 (M1 = Re, Ru) and Ni-Re-M2 (M2 = W, Ta) superalloy systems over the whole composition. Calphad: Computer Coupling of Phase Diagrams and Thermochemistry, 2021, 74, 102302.	0.7	3
662	Thermodynamic Assessment of the Ternary B-Hf-Zr System with Refined B-Hf Description. Journal of Phase Equilibria and Diffusion, 2021, 42, 864-878.	0.5	3
663	Thermodynamic Modeling of the Ge-X (X = As, Se, S, P) Systems. Journal of Electronic Materials, 2022, 51, 2114-2130.	1.0	3
664	Diffusivities and atomic mobilities in fcc Co–Cu–Mn alloys. Journal of Materials Research and Technology, 2022, 18, 5182-5196.	2.6	3
665	On the formation of λ-MnAl4. International Journal of Materials Research, 2010, 101, 611-613.	0.1	2
666	Phase equilibria in the ternary Al–Zr–La system. Journal of Alloys and Compounds, 2010, 507, 62-66.	2.8	2

#	Article	IF	CITATIONS
667	The isothermal section of Dy–Co–Cr ternary system at 500°C. Journal of Alloys and Compounds, 2011, 509, 234-236.	2.8	2
668	Mechanical Behaviors of Sic Particle Reinforced Al Matrix Composites: A Study Based on Finite Element Method. Advanced Materials Research, 2012, 535-537, 3-7.	0.3	2
669	Thermodynamic modelling and Gulliver-Scheil simulation of multi-component Al alloys. IOP Conference Series: Materials Science and Engineering, 2012, 27, 012082.	0.3	2
670	Lattice dynamics properties of XAs (X=Al, Ga and In) with zinc-blende structure from first-principle calculations. Journal of Physics and Chemistry of Solids, 2012, 73, 1034-1039.	1.9	2
671	Thermodynamic assessment of the Cd–X (X= Sr, Ti, B, V) systems. Calphad: Computer Coupling of Phase Diagrams and Thermochemistry, 2013, 42, 6-12.	0.7	2
672	Experimental investigation and thermodynamic modeling of the V–Ga system. Calphad: Computer Coupling of Phase Diagrams and Thermochemistry, 2015, 51, 125-132.	0.7	2
673	Diffusivities and Atomic Mobilities in fcc Cu-Ag-Al Alloys. Journal of Phase Equilibria and Diffusion, 2015, 36, 510-517.	0.5	2
674	Diffusivities, atomic mobilities, and simulation of ternary eutectic solidification in the Ag–Al–Cu melts. Journal of Materials Science, 2016, 51, 5979-5991.	1.7	2
675	Experimental investigation and thermodynamic modeling of the La–Mg system. Journal of Alloys and Compounds, 2016, 663, 279-288.	2.8	2
676	Experimental study on phase relationships in the Co-rich portion of the Co–Ti–Zr system. International Journal of Materials Research, 2016, 107, 217-228.	0.1	2
677	Improved ADI Scheme for Linear Hyperbolic Equations: Extension to Nonlinear Cases and Compact ADI Schemes. Journal of Scientific Computing, 2017, 72, 500-521.	1.1	2
678	Phase Equilibria of the Co-Mo-Zr Ternary System at 1100°C. Journal of Phase Equilibria and Diffusion, 2017, 38, 552-560.	0.5	2
679	Thermodynamic Calculation of Liquidus Projection of Multiple Aluminum Alloys. Materials Science Forum, 2018, 913, 589-595.	0.3	2
680	Experimental measurements of the interdiffusivities in fcc Co–rich Co–Ti, Co–W and Co–Ti–W systems. International Journal of Refractory Metals and Hard Materials, 2018, 71, 153-159.	1.7	2
681	Thermodynamic description of phase equilibria in the C–Mo–W–N quaternary system. Calphad: Computer Coupling of Phase Diagrams and Thermochemistry, 2018, 62, 201-206.	0.7	2
682	Reviews on Modeling of Diffusion-Induced Mass Transportation in Functionally Graded Cemented Carbides. , 2018, 15, 65-96.		2
683	Experimental isothermal section of the Nb-Ni-Ru ternary system at 1100â€ [−] °C. Journal of Alloys and Compounds, 2019, 810, 151801.	2.8	2
684	Evolutions of the microstructure, texture and mechanical properties of a cold rolled Al-0.8Mg-0.8Si-0.66Cu-0.1Fe-0.12Cr alloy. Materials Research Express, 2019, 6, 106564.	0.8	2

#	Article	IF	CITATIONS
685	Thermodynamic Modeling of the B-Ti-Zr System Over the Whole Composition and Temperature Ranges. Journal of Phase Equilibria and Diffusion, 2019, 40, 364-374.	0.5	2
686	Experimental study of the Be-C phase diagram. Calphad: Computer Coupling of Phase Diagrams and Thermochemistry, 2019, 64, 11-15.	0.7	2
687	Thermal stability of ternary compounds in the Cu-Li-Sn system and phase transition of the Cu6Sn5 electrode: First-principles calculations and experiment. Journal of Alloys and Compounds, 2019, 783, 44-54.	2.8	2
688	Effect of NbC on the microstructure, mechanical properties, and oxidation resistance of Ti(C,N)-based cermets. International Journal of Materials Research, 2020, 111, 479-490.	0.1	2
689	Measurement of the phase equilibria in the Al–Zr–Y system at 673 and 823ÂK. Calphad: Computer Coupling of Phase Diagrams and Thermochemistry, 2020, 68, 101726.	0.7	2
690	Experimental investigation and thermodynamic assessment of the Mn–Zr system. Calphad: Computer Coupling of Phase Diagrams and Thermochemistry, 2021, 72, 102243.	0.7	2
691	First-principles study of Mn antisite defect in Li2MnO3. Journal of Physics Condensed Matter, 2021, 33, 415201.	0.7	2
692	Interdiffusion and atomic mobilities in bcc V–X (X = Mn, Sn and Ni) alloys: Measurement and modeling. Calphad: Computer Coupling of Phase Diagrams and Thermochemistry, 2021, 74, 102316.	0.7	2
693	Thermodynamic databases and software: past, present and future. Scientia Sinica Chimica, 2019, 49, 966-977.	0.2	2
694	Thermodynamic Perspective: Insights into the Capacity Increase Phenomenon and Regulation of the Capacity Tendency of MnO for Lithium-Ion Battery Anodes. ACS Applied Energy Materials, 2021, 4, 12662-12670.	2.5	2
695	Preparation of a novel dual structure graded cemented carbides induced by bidirectional diffusion. Materials Letters, 2022, , 131689.	1.3	2
696	A First-Principles Study of the Cu-Containing β″ Precipitates in Al-Mg-Si-Cu Alloy. Materials, 2021, 14, 7879.	1.3	2
697	Experimental investigation and thermodynamic calculation in the Al–Be–Si ternary system. International Journal of Materials Research, 2022, 96, 1301-1307.	0.1	2
698	Remanufacturing of the waste refractory Mo–10Nb sputtering target by spark plasma sintering technology. Vacuum, 2022, 200, 111050.	1.6	2
699	Effect of Al content on the structural stability of Σ3 (111) twin boundary in Ti1-xAlxN hard coatings: A first-principles study. Surface and Coatings Technology, 2022, 439, 128454.	2.2	2
700	Revealing the role of Mn/Li disordered mixing in Li-rich cathode <mml:math xmlns:mml="http://www.w3.org/1998/Math/MathML"><mml:mrow><mml:msub><mml:mi>Li</mml:mi><mml:m by first-principles calculations. Physical Review Materials, 2022, 6, .</mml:m </mml:msub></mml:mrow></mml:math 	n> @. ¢mm	l:m2n>
701	Diffusion coefficients and atomic mobilities in fcc Ag–Ge and Cu–Ge alloys: Experiment and modeling. Calphad: Computer Coupling of Phase Diagrams and Thermochemistry, 2022, 78, 102453.	0.7	2
702	Interfacial Reactions Between Ain Substrate And 4-A Family Elements. Materials Research Society	0.1	1

Symposia Proceedings, 1995, 398, 269.

0.1

#	Article	IF	CITATIONS
703	Cage-like structure and charge hollow in the immiscible Cu–Ta system. Solid State Communications, 2009, 149, 1974-1977.	0.9	1
704	Mechanically driven alloying forces in the fabrication of a Cr–Zr nanocomposite. Philosophical Magazine Letters, 2011, 91, 328-336.	0.5	1
705	Phase diagram of the Al–Dy–Zr ternary system at 773 K. International Journal of Materials Research, 2012, 103, 853-857.	0.1	1
706	The electronic, mechanical and lattice dynamic properties of TiSiY from first-principles calculations. Computational Materials Science, 2012, 65, 485-489.	1.4	1
707	Phase equilibria of the Al–Mn–Zn system at 600°C. Journal of Alloys and Compounds, 2013, 556, 296-306.	2.8	1
708	Applications of TEM and 3DAP to Measurement of Phase Diagrams. Journal of Phase Equilibria and Diffusion, 2014, 35, 519-520.	0.5	1
709	Phase Field Modeling of Solute Trapping in a Al-Sn Alloy during Rapid Solidification. Materials Science Forum, 0, 794-796, 740-745.	0.3	1
710	Application of locally one-dimensional semi-implicit scheme in phase-field equations. Computer Physics Communications, 2015, 192, 148-155.	3.0	1
711	Experimental investigation of the phase equilibria in the Co–Fe–Ti ternary system. International Journal of Materials Research, 2015, 106, 841-851.	0.1	1
712	Experimental investigation and thermodynamic calculation of the Mg–Sr–Zr system. International Journal of Materials Research, 2016, 107, 534-543.	0.1	1
713	The thermochemistry of some 5:3 binary lanthanide–lead compounds by high temperature direct synthesis calorimetry. Journal of Alloys and Compounds, 2016, 656, 88-93.	2.8	1
714	Phase Equilibria of the Co-Mo-Zr Ternary System at 1000°C. Journal of Phase Equilibria and Diffusion, 2018, 39, 510-518.	0.5	1
715	Diffusion equations expressed in molar fractions: Theory and application to ionic diffusion and demixing. Physical Review E, 2019, 100, 042124.	0.8	1
716	Thermodynamic description and solidified microstructure of the Co-Ge system. Journal of Alloys and Compounds, 2019, 793, 480-491.	2.8	1
717	Thermodynamic Description of the C-Cr-Zr System Over the Whole Composition and Temperature Ranges. Journal of Phase Equilibria and Diffusion, 2020, 41, 870-882.	0.5	1
718	Quantified effect of sample size and gas environment on precipitation of an aged Al-Mg-Si alloy. Materials Characterization, 2021, 172, 110829.	1.9	1
719	Effect of (Ti, Nb)(C, N) solid-solution powder on microstructure and mechanical properties of Ti(C,) Tj ETQq1 1 0.7 2021, 8, 086518.	784314 rg 0.8	gBT /Overlo 1
720	Interdiffusion coefficients and atomic mobilities in fcc Cu-Fe-Mn alloys. Journal of Mining and Metallurgy, Section B: Metallurgy, 2014, 50, 93-99.	0.3	1

#	Article	IF	CITATIONS
721	Improved mechanical properties of dense β-Si3N4 ceramics fabricated by spark plasma sintering with Al2O3-YSZ additives. Processing and Application of Ceramics, 2018, 12, 313-318.	0.4	1
722	Thermodynamic Calculation of the Liquidus Projections of the Al-Cu-Fe-Si and Al-Cu-Fe-Mg-Si Multicomponent Systems on Al-Rich Side. Materials Science Forum, 0, 993, 984-995.	0.3	1
723	A thermodynamic description of the B–Co system: modeling and experiment. International Journal of Materials Research, 2022, 93, 1157-1163.	0.1	1
724	Temperature-dependent structural, thermal, and mechanical properties of Mo-10Nb joints prepared by SPS. Journal of Materials Science, 2022, 57, 5315-5333.	1.7	1
725	A multiple loops machine learning framework to predict the properties of WC–Co based cemented carbides. International Journal of Refractory Metals and Hard Materials, 2022, 104, 105798.	1.7	1
726	Ab initio molecular dynamics study on disordered Li-Ga-Sn system. Physical Chemistry Chemical Physics, 2022, , .	1.3	1
727	Diffusivities and atomic mobilities in the Ni-rich fcc Ni–Al–Cu alloys: experiment and modeling. International Journal of Materials Research, 2022, 113, 351-371.	0.1	1
728	First-principles studies on cation point defects in LiTi2O4. Physica B: Condensed Matter, 2022, 639, 413959.	1.3	1
729	Isothermal Section at 1000 °C of the Nb—Ti—Si System ChemInform, 2005, 36, no.	0.1	0
730	Phase Equilibria of the Fe—Nb—Ti System at 900 °C ChemInform, 2005, 36, no.	0.1	0
731	Phase Equilibria of the Cu—Nb—Ti System at 850 °C ChemInform, 2005, 36, no.	0.1	0
732	Microstructural evolution of Al–Ni–Y powders with different sizes. International Journal of Materials Research, 2005, 96, 83-88.	0.8	0
733	1 st Sino-German Symposium on Computational Thermodynamics and Kinetics and their Applications to Solidification. International Journal of Materials Research, 2008, 99, 580-581.	0.1	0
734	Iron – Silicon – Vanadium. Landolt-Bâ^šâ^,rnstein - Group IV Physical Chemistry, 2009, , 579-604.	0.0	0
735	Effect of cyclic heat treatment on the microstructures and mechanical properties of Ti–Si alloys. International Journal of Materials Research, 2010, 101, 765-771.	0.1	0
736	Mechanical Behavior of SiC Fiber Reinforced Al Matrix Composites: A Study Based on Finite Element Method. Advanced Materials Research, 0, 239-242, 2785-2789.	0.3	0
737	Experimental investigation and thermodynamic assessment of the Hf–Ge system. Journal of Materials Science, 2014, 49, 1306-1316.	1.7	0
738	CSUDDCC2: An Updated Diffusion Database for Cemented Carbides. Minerals, Metals and Materials Series, 2017, , 169-179.	0.3	0

#	Article	IF	CITATIONS
739	Microstructure and Properties of TiC Steel-Bonded Carbide Used Fe/Mo Pre-Alloyed Powder as Binder. Materials Science Forum, 0, 898, 1459-1467.	0.3	0
740	Thermodynamic assessment of the C–Nb–V ternary system over the whole composition and temperature ranges. Calphad: Computer Coupling of Phase Diagrams and Thermochemistry, 2020, 71, 102199.	0.7	0
741	Thermodynamic Calculation of the Liquidus Projections of the Al-Cu-Fe-Mg, Al-Cu-Mg-Si, and Al-Fe-Mg-Si Quaternary Systems on Al-Rich Corner. Materials Science Forum, 0, 993, 1031-1042.	0.3	0
742	Thermodynamic description, hardness and electrical conductivity of the Bi–Ni–Zn system: Experiment and modeling. Journal of Alloys and Compounds, 2020, 825, 154156.	2.8	0
743	Experimental Investigation and Thermodynamic Calculation of the Be-C-Si System. Journal of Phase Equilibria and Diffusion, 2021, 42, 515-523.	0.5	0
744	Development of Gradient Cemented Carbides through ICME Strategy. , 0, , 207-212.		0
745	Developing Cemented Carbides Through ICME. Minerals, Metals and Materials Series, 2017, , 155-167.	0.3	0
746	Effect of the combined addition of TaC and NbC on the dispersity of cubic phase in ultra-fine WC–10Co–0.5Cr cemented carbides. Materials Research Express, 2020, 7, 106505.	0.8	0
747	Experimental Investigation and Thermodynamic Verification for the Phase Relation around the Îμ-Mg23 (Al, Zn)30 Intermetallic Compound in the Mg-Zn-Al System. Materials, 2021, 14, 6892.	1.3	0
748	Solidification paths and phase equilibria at 873 and 673ÂK in the Al-Er-Zr system. Journal of Alloys and Compounds, 2021, 897, 162730.	2.8	0
749	Phase diagram of the Co–Cu–Ti system at 850 [°] C. International Journal of Materials	0.1	Ο